FragFormer: A Fragment-based Representation Learning Framework for Molecular Property Prediction

Jiaxi Wang *wjx20@mails.tsinghua.edu.cn*
Department of Electronic Engineering, Tsinghua University

Yaosen Min *yaosenmin@microsoft.com*
Microsoft Research Asia

Miao Li* *miao-li@tsinghua.edu.cn*
Department of Electronic Engineering, Tsinghua University

Ji Wu* *wuji_ee@tsinghua.edu.cn*
Department of Electronic Engineering, Tsinghua University
College of AI, Tsinghua University
Beijing National Research Center for Information Science and Technology

Reviewed on OpenReview: *https://openreview.net/forum?id=9aiuB3kIjd*

Abstract

Molecular representation learning is central to molecular property prediction, which is a vital component in drug discovery. Existing methods, which mainly focus on the atom-level molecular graphs, often find it challenging to directly model the relation between fragment (substructure) and function of molecules, largely due to insufficient fragment priors. In this work, we propose a molecular self-supervised learning framework **FragFormer**, which aims to learn the representation of fragments and their contextual relationships. Given the prior that an atom can be part of multiple functional groups, we develop k-**D**egree **Ove**rlapping fragmentation (**DOVE**), which generates overlapping fragment graph by employing the iterative line graph. Besides, DOVE can preserve the connection information during the fragmentation phase compared to non-overlapping fragmentation. In the pre-training stage, we design a *nested masked fragment prediction* objective, to capture the hierarchical nature of fragments, namely that larger fragments can encompass multiple smaller ones. Based on FragFormer, we introduce a simple yet efficient *fragment-level* interpretation method **FragCAM** for the molecular property prediction results with greater accuracy. Moreover, thanks to the fragment modeling, our model is more capable of processing large molecule, such as peptides, and capturing the long-range interactions inside molecules. Our approach achieves state-of-the-art (SOTA) performance on eight out of eleven molecular property prediction datasets on PharmaBench. On long-range biological benchmark with peptide data, FragFormer can beat strong baselines by a clear margin, which shows the model's potential to generalize to larger molecules. Finally, we demonstrate that our model can effectively identify decisive fragments for prediction results on a real-world dataset[1].

1 Introduction

Finding molecules with the desired properties is one of the biggest challenges in drug discovery (Dickson & Gagnon, 2004). Using traditional wet-lab experiments to assess molecular properties is time-consuming, labor-intensive, and costly (Mullard, 2014; Simoens & Huys, 2021; Wouters et al., 2020). Machine learning models

[*] Corresponding authors.
[1] Our code is available at `https://github.com/wjxts/FragFormer`

have been developed to predict molecular properties, which can significantly reduce the cost and time (Walters & Barzilay, 2020; Wieder et al., 2020). However, the amount of data for labeled molecular properties is often limited (Guo et al., 2021) compared with the large space of pharmacologically-relevant molecules (Virshup et al., 2013), making the generalization performance of machine learning models unsatisfactory. Fortunately, a wealth of unlabeled molecular data is available (Gaulton et al., 2017; Kim et al., 2022; Sterling & Irwin, 2015). Therefore, many studies investigate self-supervised learning (SSL) methods for molecular representation learning and achieve better results than supervised learning methods (Rong et al., 2020; You et al., 2020; Zhou et al., 2023; Li et al., 2023). These SSL methods primarily focus on the atom-level molecular graphs. In pharmaceutical chemistry, fragments serve as functional groups within molecules, fundamentally influencing their properties (Guvench, 2016). Methods based on atom-level molecular graphs often suffer from over-smoothing issue (Rusch et al., 2023) and lack fragment priors (Jiang et al., 2023), making it difficult to capture the relation between fragments and the properties of molecules. Several works develop fragment-biased GNNs (Zhu et al., 2023; Bouritsas et al., 2023; Wollschläger et al., 2024) from a theoretical perspective. Nevertheless, these models primarily aim at passing certain Weisfeiler & Leman (WL) test (Zhang et al., 2023) and are not designed for molecular property prediction. There are also studies (Zhang et al., 2021b; Luong & Singh, 2023; Jiang et al., 2023) that explore the use of fragment-level molecular graphs to develop deep learning models for predicting molecular properties and achieve encouraging results. However, their molecular fragmentation methods lack overlap between fragments, overlooking the fact that a single atom can belong to different functional groups (Merlot et al., 2003). Moreover, non-overlapping fragmentation hinders their fragment graphs from distinguishing the connections between adjacent fragments. These limitations impede the model's expressivity and generalization ability. Beyond prediction accuracy, it is also important to understand the model's decision-making process. Existing interpretation methods for molecular property prediction are either atom-level (Yuan et al., 2023) or slow to achieve fragment-level interpretation (Yuan et al., 2021). In this work, we propose FragFormer, a fragment-based molecular representation learning framework to tackle the above challenges. Our contributions can be summarized as follows:

- Given the prior that an atom can be part of multiple functional groups, we propose a novel k-**D**egree **Ove**rlapping fragmentation (DOVE) method. DOVE can generate overlapping fragment graph by utilizing the iterative line graph transformation of the molecular graph and existing non-overlapping fragmentation methods. Besides, DOVE can retain the connection information in the fragmentation step compared to non-overlapping fragmentation.
- Taking the hierarchical nature of fragment into consideration, we design a nested masked fragment prediction self-supervised objective to model this prior.
- Our FragFormer consistently surpasses previous fragment-based models and achieves SOTA performance on eight out of eleven molecular property prediction datasets on PharmaBench.
- Based on the fragment modeling, our model is more capable of processing large molecules, outperforms strong baselines on long-range biological benchmark with peptide data.
- Building on fragment modeling, we introduce a simple fragment-level interpretation technique, called FragCAM, for the prediction outcomes. Our method achieves greater accuracy and faster speed on a real-world molecular property prediction dataset with labeled decisive fragments.

2 Related Works

2.1 Molecular Representation Learning

Obtaining good molecular representation is a crucial step for accurately predicting molecular properties (Tkatchenko, 2020). Conventional quantitative structure–activity relationship (QSAR) methods (Hansch et al., 1962; Tropsha, 2010) formulate a variety of handcrafted molecular descriptors to serve as fixed features for molecules. These features can be used as input for various machine learning models, such as SVM (Cortes & Vapnik, 1995), XGBoost (Chen & Guestrin, 2016), etc. Such fixed features can reflect simple substructures and physicochemical properties of molecules, but may not be able to capture the necessary and sophisticated structure feature of molecules for a specific task. To adaptively learn the molecular features, supervised deep learning methods are proposed to learn the molecular representation from the molecular graph or SMILES (Weininger, 1988) string directly with labeled data (Chen et al., 2018). These methods can effectively capture the relevant features of molecular properties and outperform traditional methods when provided with sufficient labeled data (Masters et al., 2023). However, the performance of these methods is constrained by the amount of labeled data, which is usually limited in practice (Guo et al., 2021). Owing to the success of self-supervised learning (SSL) in the field of computer vision (CV) (He et al., 2022; Chen et al., 2020b), natural language processing (NLP) (Devlin et al., 2019) and audio analysis (Baevski et al., 2020; Hsu et al., 2021), SSL methods have been proposed for learning molecular representation by harnessing the abundant unlabeled molecular data. These methods primarily fall into two categories: those based on masked autoencoders, and those that employ contrastive learning. MolBERT (Fabian et al., 2020) and MolGPT (Bagal et al., 2022) use the string representation of molecules and predict the masked tokens in the SMILES string in the pre-training stage. GraphLoG (Xu et al., 2021), GROVER (Rong et al., 2020) and GEM (Fang et al., 2021) treat the molecule as 2D graph, and predict the masked nodes in the graph with graph neural networks. KPGT (Li et al., 2023) further improves the performance by modeling the global information of the molecular graph with a transformer style architecture. Contrastive learning-based methods depend on constructing different views of the same molecule. GraphCL (You et al., 2020; 2021) achieves this by randomly dropping, perturbing, and masking parts of the molecular graph. MoleculeSTM (Liu et al., 2023) utilizes text descriptions of the molecule as an alternative view, while GraphFP (Luong & Singh, 2023) and Holi-Mol (Kim et al., 2024) employ the fragment graph of the molecule for this purpose. Although these methods have advanced the performance of molecular property prediction, they mainly focus on the atom-level molecular graphs, and often struggle to directly model the relation between fragments and molecular properties due to the lack of fragment prior, restricting their interpretability and generalization. In this work, we propose a novel overlapping fragmentation method, along with a nested masked fragment prediction pre-training task, to effectively learn the representation of fragments and their contextual relationships.

2.2 Fragment-based Molecular Learning

Fragment-based drug discovery (FBDD) is an emerging method in drug discovery (Murray & Rees, 2009). Unlike high-throughput screening (Macarron et al., 2011), FBDD focuses on the interactions between small fragments and target proteins, and extends the fragments to larger molecules with higher binding affinity. FBDD can explore the chemical space more efficiently and reduce the cost of drug discovery with higher success rate (Murray & Rees, 2009). Motivated by the success of FBDD, researchers have proposed fragment-based methods in molecular learning tasks, mostly on molecule generation. Compared with atom-based molecule generation, fragment-based methods can generate molecules more efficiently and with more validity. Most fragment-based methods in molecule generation employ a variational autoencoder (VAE) framework (Voloboev, 2024; Kingma & Welling, 2014; Jin et al., 2018; 2020; Kong et al., 2022; Yu & Yu, 2024). JT–VAE decomposes the molecule into a tree structure (Rarey & Dixon, 1998) and generates the molecule by a tree expansion. HierVAE constructs fragment with multiple properties and subsequently expand this fragment. PS–VAE employs a data-driven method to build fragment vocabulary and generate molecules one fragment at a time, which emulates the subword vocabulary construction and tokenization process in NLP (Sennrich et al., 2016). Recently, there are some studies that explore fragment-based methods for molecular property prediction (Zhang et al., 2021a;b; Luong & Singh, 2023; Jiang et al., 2023; Kim et al., 2024). Fragment-based methods take advantage of the prior that fragments are the functional groups within molecules (Guvench, 2016), which are basic building blocks in pharmaceutical chemistry. MGSSL (Zhang et al., 2021a) utilizes predefined motifs as supervision in its self-supervised learning task. FragGAT (Zhang et al., 2021b) segments the molecular graph in different ways, processes each segment with an Attentive FP network (Xiong et al., 2020), and aggregates the segment embedding to predict the molecular properties. GraphFP (Luong & Singh, 2023) employs the fragment graph of the molecule as an alternative view in contrastive learning to enhance atom-level molecular modeling. Holi-Mol(Kim et al., 2024) further utilizes multiple views of fragmentation to enrich the representation. PharmHGT (Jiang et al., 2023) integrates both fragment and atom graphs to model the molecular properties. Although existing fragment-based methods have demonstrated encouraging results in molecular property prediction and heightened the interpretability of the model, they have yet to surpass atom-level molecular graph based methods (Chen et al., 2024). We postulate that the reason is their fragmentation methods primarily focus on the non-overlapping fragmentation, which cannot model the fact that a single atom can contribute to different functional groups (Merlot et al., 2003). Besides, the non-overlapping fragmentation results in connection information loss between fragments. In the fragment graph with non-overlapping fragmentation, an edge cannot specify how two fragments are connected, as any two atoms within each fragment may serve as the connection points. In this work, we propose a novel overlapping fragmentation method with tunable overlapping degree and learnable fragment vocabulary. Our method allows a single atom to participate in multiple fragments and the overlapped atoms maintain the connection information between fragments.

2.3 Interpretation Methods for Molecular Property Prediction

Identifying the critical fragments for prediction results is essential for applying machine learning models in real-world scenarios for molecular property prediction (Proietti et al., 2024). Existing interpretation methods can be divided into two categories: atom-level and fragment-level. Atom-level interpretation methods aim to identify the important atoms for prediction results. Gradient-based attribution methods from CV, such as class activation maps (CAM) (Zhou et al., 2016), GradCAM (Selvaraju et al., 2020), GradInput (Shrikumar et al., 2017) and Integrated Gradients (IG) (Sundararajan et al., 2017), can be directly applied to score the importance of atoms in molecular property prediction tasks. Rao et al. (2021) builds a benchmark DrugXAI for interpreting molecular property prediction models and shows these methods can achieve good performance on synthetic datasets, but poor performance on real-world datasets. They also find that GradInput and IG perform better than other gradient-based methods. Many interpretation methods have been specifically developed for graph neural networks (Ying et al., 2019; Luo et al., 2020; Yuan et al., 2021). GNNExplainer (Ying et al., 2019) learns masks for node features and edges by maximizing the mutual information between the masked subgraph and the prediction. PGExplainer (Luo et al., 2020) utilizes a deep network to model the explanation generation process. While atom-level interpretation methods can highlight key atoms relevant to the predictions, they do not necessarily guarantee fragment-level explanations. SubgraphX (Yuan et al., 2021) aims to identify the most important connected subgraph for prediction results using Monte Carlo Tree Search (MCTS), offering better fragment-level interpretation compared to GNNExplainer and PGExplainer. However, it involves greater computational overhead. Existing methods either fail to guarantee fragment explanations or are slow in producing them. In this work, we propose a simple but efficient fragment-level interpretation method based on fragment modeling. Our method achieves better performance with faster speed on a real-world mutagenicity dataset.

3 Methods

In this section, we introduce our self-supervised learning framework, FragFormer, designed for molecular property prediction based on fragment modeling. The overall pipeline is depicted in Figure 1. In the following subsections, we first propose a novel overlapping fragmentation method and derive the fragment graph. Next, we introduce our model architecture, which takes fragment graph as input and produces the representation for both fragments and the whole molecule. Finally, we describe the nested masked fragment prediction pre-training, which aims to capture the hierarchical nature of fragments and their contextual relationships.

3.1 k-Degree Overlapping Fragmentation (DOVE)

Existing fragmentation methods mainly focus on non-overlapping fragmentation, which partition the molecule into disjoint atom sets (Lewell et al., 1998; Degen et al., 2008; Kong et al., 2022). The non-overlapping fragmentation methods have two drawbacks. First, one atom can only belong to one fragment, violating the fact that a single atom can be part of multiple functional groups (Merlot et al., 2003). Second, the induced fragment graph loses certain topological information from the original molecular graph. Such fragment graph cannot capture how two fragments are connected (see Appendix B for an illustration). To solve the above issues, we propose a novel method of overlapping fragmentation with learnable fragment library. It permits a single atom to participate in multiple fragments. The overlapping atoms can retain pivotal connection details between fragments, allowing for effective assembly and reducing connection information loss during the transformation from molecular graph to fragment graph. Our method is based on the iterative

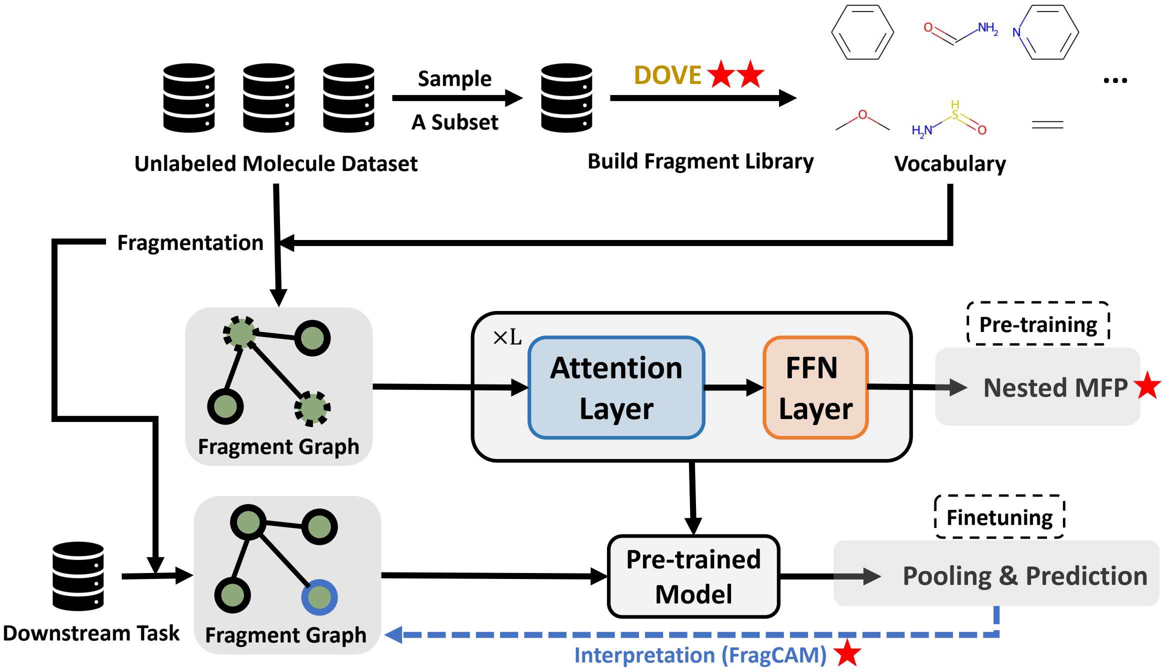

Figure 1: Pipeline of the FragFormer. "FFN": feed forward network. "MFP": masked fragment prediction. "★" represents our core design in FragFormer. We propose k-degree overlapping fragmentation (DOVE) to generate overlapping fragment graph, and nested MFP self-supervised learning to capture the hierarchical nature of fragments. FragCAM can effectively provide decisive fragments for prediction results.

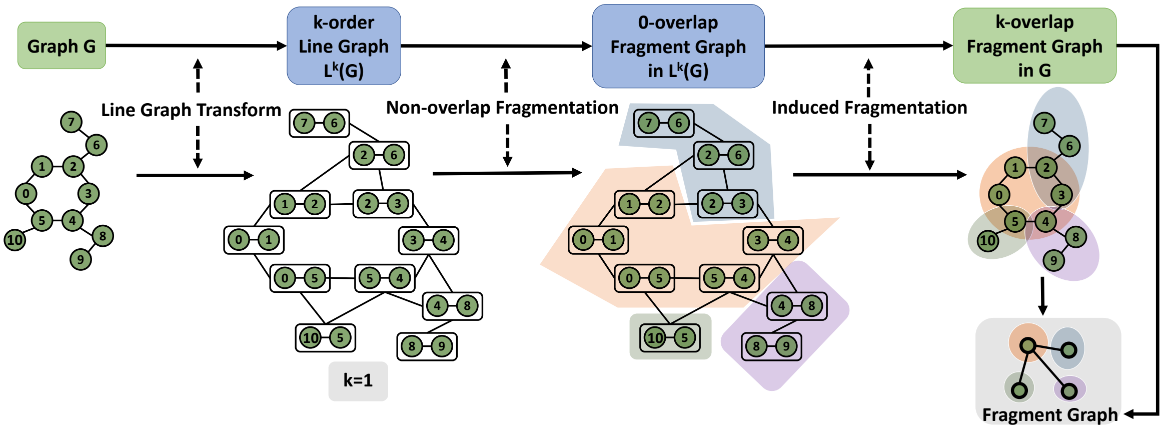
Graph G
k-order Line Graph L^k(G)
0-overlap Fragment Graph in L^k(G)
k-overlap Fragment Graph in G
Line Graph Transform
Non-overlap Fragmentation
Induced Fragmentation
k=1
Fragment Graph

Figure 2: Pipeline of the k-degree overlapping fragmentation (DOVE) with $k = 1$.

line graph transformation of the molecular graph and can take advantage of the existing non-overlapping fragmentation methods. The pipeline is shown in Figure 2. The main idea is that *the non-overlapping fragmentation of the k-order line graph can be transformed to the k-degree overlapping fragmentation of the original molecular graph.* We first formally define k-degree overlapping fragmentation and k-order line graph. Then, we show that the k-degree overlapping fragmentation of the molecular graph can be obtained by the non-overlapping fragmentation of the k-order line graph. We assume all the graphs G are undirected in the following description.

Definition 1 (Fragmentation of graph)**.** Given a graph $G = (V, E)$, $P = \{V_i\}_{i=1}^{m}$, $\mathbf{A} \in \mathbb{R}^{m\times m}$, we define $F = (P, A)$ as a fragmentation (fragment graph) of G if

1. P is a vertex cover of G, i.e, $\bigcup_{i=1}^{m} V_i = V$. P also represents the nodes in fragment graph.
2. $\forall i \in \{1, 2, \cdots, m\}$, $G[V_i]$ is a connected subgraph. $G[V_i]$ represents the subgraph restricted to vertex set V_i.

Here, $\mathbf{A}$ symbolizes the adjacency matrix for the fragment graph, indicating whether two fragments are neighbors. This adjacency is flexible and can be adjusted based on specific requirements.

Definition 2 (k-degree overlapping fragmentation)**.** Given a graph $G = (V, E)$, $P = \{V_i\}_{i=1}^{m}$, $\mathbf{A} \in \mathbb{R}^{m \times m}$, we call a fragmentation $F = (P, A)$ as a k-degree overlapping fragmentation if:

- $\forall\ i, j \in \{1, 2, \cdots, m\}, i \neq j$, if $A_{ij} = 1$, i.e., V_i and V_j are neighbors in G, then $|V_i \cap V_j| \geq k$.

Next, we define k-order line graph and show how it can be used to generate the k-degree overlapping fragmentation of the original molecular graph.

Definition 3 (Line graph transformation)**.** Given a graph $G = (V, E)$, the line graph $L(G)$ is an undirected graph whose vertices correspond to the edges of G and two vertices are connected by an edge if the corresponding edges in G share a common vertex.

We assume G is connected and leave the discussion for disconnected graph in Appendix A.

Definition 4 (k-order line graph)**.** Let $L^0(G) = G$. For integer $k \geq 1$, the k-order line graph $L^k(G)$ is defined recursively as $L^k(G) = L(L^{k-1}(G))$.

Each vertex v in $L^k(G)$ corresponds to a $(k+1)$-size connected subgraph in G. We denote its node set by $C(v)$.

Definition 5 (Standard 0-degree overlapping fragmentation)**.** Given a graph $G = (V, E)$, $P = \{V_i\}_{i=1}^{m}$, $\mathbf{A} \in \mathbb{R}^{m \times m}$, we call a fragmentation $F = (P, A)$ as a standard 0-degree overlapping fragmentation if:

1. $\forall\ i, j \in \{1, 2, \cdots, m\}, i \neq j$, we have V_i and V_j are disjoint, i.e, $|V_i \cap V_j| = 0$.
2. $A_{ij} = 1$ if there exists node $v_i \in V_i$ and $v_j \in V_j$, such that v_i and v_j are neighbors in G, otherwise $A_{ij} = 0$.

Most commonly used fragmentation methods are standard 0-degree overlapping fragmentation, such as principal subgraph mining (Kong et al., 2022), BRICS (Degen et al., 2008) and Recap (Lewell et al., 1998).

Definition 6 (Induced fragmentation)**.** Given a graph $G = (V, E)$ and a fragmentation $F = (P, A)$ of $L^k(G)$, where $P = \{U_i\}_{i=1}^{m}$, $\mathbf{A} \in \mathbb{R}^{m \times m}$, the induced fragmentation of F is defined as $F' = (Q, A)$, where $Q = \{V_i\}_{i=1}^{m}$, $V_i = \bigcup_{v \in U_i} C(v)$.

Theorem 1. *Given a graph $G = (V, E)$, the induced fragmentation of standard 0-degree overlapping fragmentation of $L^k(G)$ is a k-degree overlapping fragmentation of G.*

The proof can be found in Appendix A. By Theorem 1, we first transform the molecular graph to the k-order line graph, then use existing graph fragmentation method to get the standard 0-degree overlapping fragmentation of $L^k(G)$, and finally get the k-degree overlapping fragmentation of G by the induced fragmentation. The overlapping degree can be controlled by adjusting the order k of the line graph. We apply principal subgraph mining (Kong et al., 2022) as our standard 0-degree overlapping fragmentation method, which can generate a succinct and fruitful fragment vocabulary.

3.2 Model Architecture of FragFormer

Assume the fragmentation of the molecular graph is $F = (P, \mathbf{A})$, where $P = \{V_i\}_{i=1}^{m}$ is the fragment set and $\mathbf{A}$ is the fragment adjacent matrix. The architecture of FragFormer is designed to model the contextual relationships among fragments and to learn the representation of those fragments. The model architecture of FragFormer consists of three main components: subgraph encoder, fragment-level graph transformer and knowledge-aware fusion. The overall architecture is shown in Figure 3.

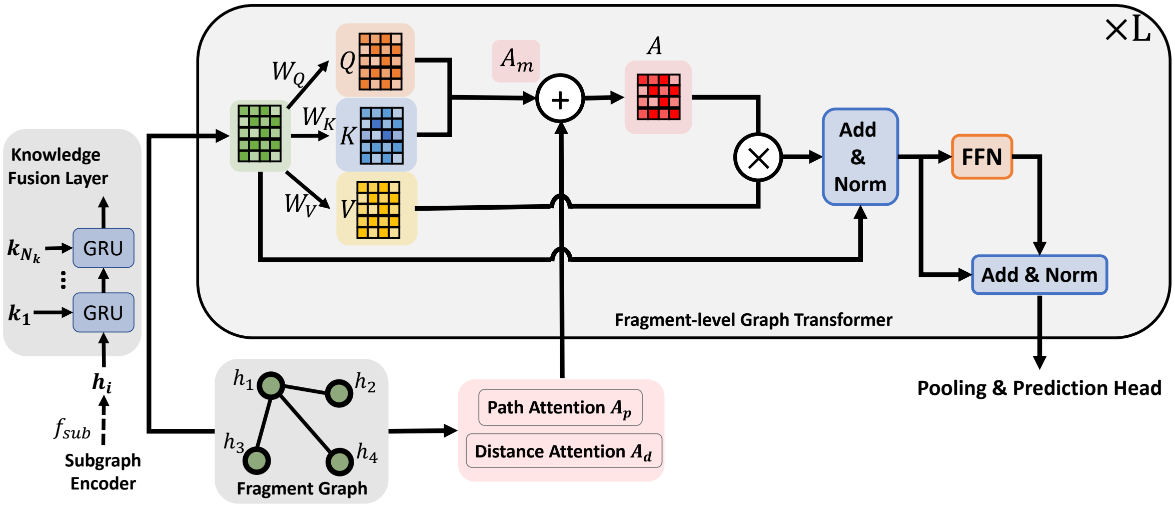

Figure 3: Model architecture of FragFormer.

Subgraph Encoder

Given a fragment V_i in the overlapping fragmentation, we first obtain the embedding $\mathbf{h}_i$ of fragment V_i by using a subgraph encoder f_{sub}:

$$\mathbf{h}_i = f_{sub}(G[V_i]).$$

$\{\mathbf{h}_i\}_{i=1}^m$ serve as the node features in the fragment graph.

Fragment-level Graph Transformer

Using fragment embeddings $\{\mathbf{h}_i\}_{i=1}^m$ and $\mathbf{A}$, we apply a transformer-based architecture (Vaswani et al., 2017) that operates on the fragment graph to model contextual dependency between fragments and learn a graph-level representation for molecular property prediction.

Fragment-level graph transformer is composed of L graph transformer layers, each of which consists of a self-attention mechanism and a feed-forward module. We follow the design of self-attention mechanism in Li et al. (2023); Ying et al. (2021); Shi et al. (2022), which includes path attention and distance attention as a reflection of graph topology.

Specifically, given the fragment graph and fragment features $\mathbf{H}^l \in \mathbb{R}^{d\times m}$ at the l-th layer, where d is the dimension of the feature and m is the number of fragments, the self attention is calculated as:

$$\mathbf{Q} = \mathbf{W^Q}\mathbf{H}^l,\ \mathbf{K} = \mathbf{W^K}\mathbf{H}^l,\ \mathbf{V} = \mathbf{W^V}\mathbf{H}^l,$$

$$\mathbf{A} = \text{softmax}\left(\frac{\mathbf{K^T}\mathbf{Q}}{\sqrt{d}} + \mathbf{A^d} + \mathbf{A^p}\right),$$

$$\mathbf{H}^{l+\frac{1}{2}} = \text{LayerNorm}\left(\mathbf{VA} + \mathbf{H}^l\right),$$

$\mathbf{W^Q}$, $\mathbf{W^K}$ and $\mathbf{W^V} \in \mathbb{R}^{d\times d}$ are projection weight matrices for query ($\mathbf{Q}$), key ($\mathbf{K}$) and value matrix $\mathbf{V}$.

$\mathbf{A^d}$ and $\mathbf{A^p}$ are distance attention and path attention. Assume the distance between fragment i and fragment j in fragment graph is N_p, and the shortest path between fragment i and fragment j is $p_{ij} = (i_0, \ldots, i_{N_p})$, then $\mathbf{A^d}$ and $\mathbf{A^p}$ are computed as:

$$A^d_{ij} = c_{N_p},$$

$$A^p_{ij} = \frac{1}{N_p}\sum_{k=0}^{N_p} \mathbf{W}^p_k \mathbf{h}_{i_k},$$

where c_{N_p} is a learnable scalar, $\mathbf{W}_k^p \in \mathbb{R}^{d\times 1}$ is a learnable weight matrix. The feed forward module is defined as:

$$\mathbf{H}^{l+1} = \text{LayerNorm}\left(\text{FFN}(\mathbf{H}^{l+\frac{1}{2}}) + \mathbf{H}^{l+\frac{1}{2}}\right),$$

where FFN is a two-layer MLP with ReLU activation (Agarap, 2018). The initial feature $\mathbf{H}^0$ is the fragment embedding $\{\mathbf{h}_i\}_{i=1}^m$. The output feature $\mathbf{H}^L$ is the final fragment representation. At last, we apply a global pooling operation on $\mathbf{H}^L$ to obtain the graph-level representation $\mathbf{h}_G$.

Knowledge Fusion Layer

Incorporating fixed substructure-related features, such as extended connectivity fingerprints (ECFP) (Rogers & Hahn, 2010), are beneficial for molecular representation learning (Li et al., 2023; Rong et al., 2020). We refer to those fixed features as knowledge vectors. Here, we propose a knowledge fusion layer to incorporate the knowledge vectors into the fragment representation learning. We integrate the knowledge vector $\mathbf{k}$ with the fragment representation $\mathbf{h}_i$ through a GRU unit (Xiong et al., 2020) right after the subgraph encoder:

$$\mathbf{h}_i \leftarrow \text{GRU}\left(\mathbf{k}, \mathbf{h}_i\right).$$

If there are multiple knowledge vectors $\{\mathbf{k}_i\}_{i=1}^{N_k}$, we sequentially integrate them with the fragment representation, as illustrated in the bottom left corner of Figure 3.

3.3 Nested Masked Fragment Prediction Pre-training

To distill knowledge from massive unlabeled molecular data, it is essential to pre-train the model with a self-supervised objective. Here, we propose a novel fragment-based pre-training task, which is designed to model the hierarchical nature of fragments. Several atoms can assemble into small fragments, and a combination of these small fragments can constitute larger ones. Our design follows the philosophy of mask autoencoder (Devlin et al., 2019; He et al., 2022), where we mask the fragment nodes and predict the masked nodes based on the context. Instead of barely predicting the class label of the masked nodes, we predict the existence of all substructures in the vocabulary V for the masked nodes. We use a 0-1 vector $\mathbf{y} \in \mathbb{R}^{|V|}$ to represent the existence of the substructure in the vocabulary. $y_i = 1$ if the i-th substructure exists in the masked node, otherwise $y_i = 0$. We predict the existence of the substructure by using a linear classifier built on the fragment representation $\mathbf{h}^L$ and a binary cross entropy loss:

$$\mathcal{L} = -\sum_{i=1}^{|V|} y_i \log\left(\text{sigmoid}\left(\mathbf{w}_i^T \mathbf{h}^L\right)\right) + (1-y_i)\log\left(1 - \text{sigmoid}\left(\mathbf{w}_i^T \mathbf{h}^L\right)\right).$$

3.4 Fragment-level Interpretation: FragCAM

Inspired by the class activation mapping (Zhou et al., 2016) in CV, we combine it with our fragment modeling and propose **Frag**ment **C**lass **A**ctivation **M**apping (FragCAM) for explaining the prediction results with fragments. Assume the final fragment representation is $\left\{\mathbf{h}_i^L\right\}_{i=1}^m$ and we predict the molecular property with a linear classifier $\mathbf{w} \in \mathbb{R}^d$:

$$\hat{y} = \mathbf{w}^T \text{SumPooling}\left(\left\{\mathbf{h}_i^L\right\}_{i=1}^m\right).$$

Then, the attribution of the i-th fragment to the prediction result is calculated as:

$$\text{Attribution}_i = \frac{\mathbf{w}^T \mathbf{h}_i^L - \text{Min}}{\text{Max} - \text{Min}},$$

where Max and Min are the maximum and minimum value of $\left\{\mathbf{w}^T \mathbf{h}_i^L\right\}_{i=1}^m$, respectively.

4 Experiments

4.1 Pre-training

Dataset We use two millions unlabeled molecular SMILES (Weininger, 1988) from CHEMBL29 (Gaulton et al., 2017) as our pre-training data. We use RDKit (Landrum, 2016) to generate the molecular graph from

Table 1: Results on PharmaBench. The best results are in bold. "↑" means the higher the better, while "↓" means the lower the better. FragFormer can achieve the SOTA preformance on eight out of eleven tasks. "‡" indicates traditional QSAR method. "$*$" means the methods include a pre-training stage. Baselines labeled with "†" are fragment-based methods. The best performance of previous baseline methods (annotated with underlines) on each dataset mostly comes from methods based on atomic graphs.

	Classfication (AUROC ↑)		Regression (RMSE ↓)								
Model/Dataset	AMES	BBB	CYP2C9	CYP2D6	CYP3A4	HLMC	MLMC	RLMC	LogD	PPB	Sol
RF‡ (Breiman, 2001)	0.761	0.731	18.471	18.041	16.540	0.813	0.987	0.958	1.249	0.204	0.918
XGBoost‡ (Chen & Guestrin, 2016)	0.768	0.750	17.582	17.819	16.123	0.647	0.844	0.819	1.071	0.186	0.832
CMPNN (Song et al., 2020)	0.858	0.887	18.377	19.156	16.701	0.921	1.130	0.939	0.807	0.236	0.858
FPGNN (Cai et al., 2022)	0.858	0.923	16.933	17.611	15.606	0.604	0.774	0.716	0.838	0.179	0.747
DHTNN (Song et al., 2023)	0.844	0.909	17.449	17.890	16.156	0.729	0.926	0.915	0.912	0.235	0.828
KANO* (Fang et al., 2023)	0.865	0.915	17.350	17.622	15.307	0.554	0.767	0.762	0.766	0.185	0.772
MPG* (Li et al., 2021)	0.869	0.923	17.417	17.527	**14.376**	0.541	0.723	0.685	0.758	0.170	0.758
Unimol* (Zhou et al., 2023)	0.878	0.920	17.774	18.071	15.895	0.613	0.824	0.651	0.745	0.179	**0.707**
Trans-M* (Luo et al., 2023)	0.869	**0.935**	18.080	17.677	15.867	0.567	0.744	0.677	0.737	0.172	0.834
KPGT* (Li et al., 2023)	0.880	**0.935**	17.036	16.860	16.379	0.564	0.726	0.881	0.728	0.172	1.221
GraphFP*† (Luong & Singh, 2023)	0.830	0.893	17.367	21.183	17.219	0.764	0.878	0.771	0.835	0.208	1.935
FraGAT† (Zhang et al., 2021b)	0.778	0.684	17.788	22.503	20.313	0.775	0.849	1.050	0.945	0.220	1.352
PharmHGT† (Jiang et al., 2023)	0.863	0.913	17.490	15.020	16.077	0.544	0.820	0.677	0.676	0.172	0.954
FragFormer-0*† (ours)	0.868	0.920	18.094	17.096	17.036	0.624	0.875	0.619	0.774	0.190	0.968
FragFormer-1*† (ours)	**0.889**	0.928	**16.855**	**14.425**	15.894	**0.514**	0.702	0.596	**0.667**	**0.157**	0.895
FragFormer-2*† (ours)	0.870	0.921	17.017	14.505	15.708	0.525	**0.688**	**0.541**	0.670	0.177	0.901
FragFormer-3*† (ours)	0.870	0.918	17.835	16.780	16.977	0.545	0.732	0.571	0.714	0.193	0.961

SMILES and extract the atom features with 137 dimension. The detailed description of atom featurization can be found in Appendix D. We randomly sample $100k$ molecules to generate the fragment vocabulary by principal subgraph mining (Kong et al., 2022). We set the vocabulary size as 500 for the vocabulary constructon. We separately generate the library for different degree of overlapping fragmentation. The higher the degree of overlapping, the slower the vocabulary construction and molecule fragmentation. We select the degree of overlapping from $\{0, 1, 2, 3\}$ in our experiments. FragFormer with k-degree overlapping fragmentation is denoted as FragFormer-k. For the knowledge fusion layer, we extract ECFP (Rogers & Hahn, 2010) with radius = 2 and 1024 bits, MACCS (Durant et al., 2002), TorsionFP (Schulz-Gasch et al., 2012), and physic-chemical descriptors (Yang et al., 2019; Xue & Bajorath, 2000) as the knowledge vectors. We linearly transform the raw knowledge vectors to the same dimension as the fragment representation with a learnable projection for each kind of knowledge before the fusion.

Training Details We use $L = 6$ graph transformer layers in FragFormer with model dimension $d = 512$. We use a two-layer Graph IsoMorphism Network (GIN) (Xu et al., 2019) with mean pooling and hidden dimension d as the subgraph encoder f_{sub}. We use batch size $bs = 4096$, learning rate $lr = 2e - 4$, and Adam optimizer (Kingma & Ba, 2015) with $(\beta_1, \beta_2) = (0.9, 0.999)$ in the stochastic training. We apply linear learning rate decay scheduler with $5k$ warm-up steps. We totally train the model for $25k$ steps on 4 NVIDIA 4090 GPUs. The masked fragment ratio is set as 0.3. The attention dropout rate and feed forward dropout rate are set as 0.1 in all fragment-level graph transformer layer. We adopt the multi-head attention technique with 8 heads in each layer (Vaswani et al., 2017). In the fine-tuning stage, we add a sum pooling on top of the pre-trained model and apply a linear predictor at last. More detailed description can be found in Appendix D.

4.2 Downstream Tasks

We test our method on molecular ADMET (Absorption, Distribution, Metabolism, Excretion, and Toxicity) property prediction benchmark PharmaBench (Niu et al., 2024), long-range biological benchmark (Dwivedi et al., 2022b), and interpretability benchmark DrugXAI for molecular property prediction (Rao et al., 2021).

PharmaBench PharmaBench (Niu et al., 2024) is a comprehensive benchmark for predicting molecular ADMET properties, featuring eleven distinct molecular property prediction tasks curated with the assistance of a multi-agent large language model system. The benchmark encompasses a total of 52,482 entries drawn from 14,401 bioassays, including two classification tasks and nine regression tasks. The detailed profile of the tasks can be found in the Appendix D. We follow the same scaffold splitting setting (Yang et al., 2019) in PharmaBench which divides the dataset into training and test sets with a ratio of 4:1. We compare our method with traditional QSAR methods, atom-based methods and fragment-based methods. For traditional QSAR methods, we use ECFP descriptors with radius 2 and 1024 bits. For classification and regression tasks, we use AUROC and root mean square error (RMSE) as evaluation metrics, respectively. We report the mean performance of three runs with different random seeds.

Long-range Biological Benchmark To assess the model's generalization preformance on large molecules and its capacity to capture long-range interactions, we evaluate it using the peptides-func datatset from the Long Range Graph Benchmark (Dwivedi et al., 2022b)[2] which predicts 10 biological functions of peptide data, e.g., Antibacterial, Antiviral, cell-cell communication, and others. This benchmark is designed to test the model's ability to model long range interactions between atoms. We compare our method with both graph convolutional based methods (Kipf & Welling, 2017; Chen et al., 2020a; Hu et al., 2020; Bresson & Laurent, 2017), transformer-based methods (Kreuzer et al., 2021) and fragment-based methods (Luong & Singh, 2023). Due to the large GPU memory cost for large molecule, we reduce the model dimension d to 32 in this benchmark. We report the average precision (AP) for the benchmark with three different runs.

DrugXAI Apart from the performance on molecular property prediction, explainability is also crucial for the model to be deployed in real-world applications. We evaluate our interpretation method FragCAM on DrugXAI (Rao et al., 2021). We choose two synthetic datasets and one real-world dataset from DrugXAI. Detailed descriptions of the datasets can be found in the Appendix C. Two synthetic datasets predict the existence of 3MR and Benzene substructures in the molecule, respectively. The ground truth attribution fragment is the corresponding substructure. The real-world dataset aims at predicting the ames mutagenicity. We use the 46 substructure alerts given by Sushko et al. (2012) as ground truth fragments. Following DrugXAI, we use AUROC metric proposed by McCloskey et al. (2019) to measure the model preformance, which computes the macro average AUROC between the predicted attribution and the ground truth attribution across test molecules. To evaluate FragCAM, we convert the fragment attribution into atom attribution by assigning the attribution of the fragment to the atoms it contains. If one atom is present in multiple fragments, we assign it the maximum attribution from those fragments. We compare our method with both atom-based and subgraph-based attribution approaches. For the atom-based methods, we adhere to the baseline settings established in DrugXAI. We apply CAM (Zhou et al., 2016), GradCAM (Selvaraju et al., 2020), GradInput (Shrikumar et al., 2017), and IG (Sundararajan et al., 2017) to CMPNN (**?**), GraphSAGE (Hamilton et al., 2017a), GraphNet (Battaglia et al., 2018), and GAT (Velickovic et al., 2018). We report the best results among the four atom-based attribution methods for each model. For subgraph-based method, we use SubgraphX (Yuan et al., 2021) on a two-layer GCN (Kipf & Welling, 2017) with dimension d. In SubgraphX, we set the target number of fragment nodes N_{min} from $\{3, 7, 10, 15\}$, use 20 rollouts in MCTS, and apply 20 steps in shapley value estimation. We also report the fidelity and sparsity score (Pope et al., 2019; Yuan et al., 2023) for fragment attribution. The fidelity metric evaluates how accurately the explanations reflect the model's decision-making process. It removes the crucial substructures from the input graphs and analyze the variation in predictions. The sparsity metric quantifies the proportion of structures ignored by the explanation methods. Higher fidelity under similar or lower sparsity are preferred.

4.3 Results and Discussions

PharmaBench The model performance on PharmaBench is presented in Table 1. Firstly, it is noteworthy that FragFormer achieves the SOTA performance in eight out of eleven tasks. Secondly, it consistently outperforms fragment-based baselines (indicated with †) with clear margins across all tasks. Thirdly, FragFormer employing overlapping fragmentation ($k = 1$ or $k = 2$) exhibits substantially superior performance in contrast to the non-overlapping fragmentation ($k = 0$). Excessive overlapping ($k = 3$) lead to performance degradation. We recommend using $k = 1$ or $k = 2$ for optimal results. These outcomes substantiate the efficiency of the FragFormer framework, particularly in context to its overlapping fragmentation feature. However, our method still falls short of atom-based pre-training methods on three tasks, which we aim to address in future work. We also find that for each task, the best method always involves a pre-training stage, which highlights the importance of pre-training in molecular property prediction.

[2] There is another peptide dataset called peptides-struct in the benchmark. However, peptides-struct pays attention to predicting the geometric quantities of peptides, which is beyond the scope of our work.

Table 2: Results on long-range biological benchmark. "w.o KF": without knowledge fusion layer.

Model	**# Params.**	**Test AP (↑)**
GCN (Kipf & Welling, 2017)	508k	0.5930±0.0023
GCNII (Chen et al., 2020a)	505k	0.5543±0.0078
GINE (Hu et al., 2020)	476k	0.5498±0.0079
GatedGCN (Bresson & Laurent, 2017)	509k	0.5864±0.0077
GatedGCN (Bresson & Laurent, 2017)+RWSE (Dwivedi et al., 2022a)	506k	0.6069±0.0035
GraphFP (Luong & Singh, 2023)	2.5M	0.6267±0.0073
Transformer (Vaswani et al., 2017)+LapPE (Dwivedi et al., 2020)	488k	0.6326±0.0126
SAN (Kreuzer et al., 2021)+LapPE (Dwivedi et al., 2020)	493k	0.6384±0.0121
SAN (Kreuzer et al., 2021)+RWSE (Dwivedi et al., 2022a)	500k	0.6439±0.0075
FragFormer (w.o KF)	500k	**0.6571±0.0104**
FragFormer	2M	**0.6693±0.0154**

Table 3: Performance (AUROC) results on DrugXAI. The best results are in bold. For CMPNN, GraphSAGE, GraphNet, and GAT, we report the best results among CAM, GradCAM, GradInput, and IG.

Dataset/Model	CMPNN	GraphSAGE	GraphNet	GAT	FragCAM
3MR	0.966	0.932	0.967	0.905	**0.981**
Benzene	0.906	0.859	0.934	0.867	**0.935**
Mutagenicity	0.742	0.742	0.759	0.683	**0.793**

Long-range Biological Benchmark We show the results on the long-range biological benchmark in Table 2. FragFormer without knowledge fusion layer has the same amount of parameters as the baselines and outperforms the best baseline by more than 1% in terms of test AP. Compared to another fragment-based method GraphFP, FragFormer contains less parameters, but achieves a absolute improvement of 4.26% in test AP. These results demonstrate the effectiveness of FragFormer in processing large molecule and modeling long-range interactions in biological data.

Interpretability Benchmark DrugXAI The results on DrugXAI are displayed in Table 3 and Table 4. In Table 3, FragCAM can significantly outperform the atom-based methods for baseline models on 3MR and mutagenicity dataset. For Benzene, FragCAM can also achieve competitive performance among all models. Compared to SubgraphX, FragCAM demonstrates superior AUROC and fidelity while achieving significantly faster speeds on the mutagenicity dataset. We also visualize the FragCAM results on mutagenicity datasets in Figure 4. FragCAM can accurately locate the nitro group, diazene and epoxyethane group as alerts for ames mutagenicity. These results demonstrate the effectiveness of FragCAM in explaining the prediction results with fragments.

4.4 Ablation Study

In this section, we use the PharmaBench dataset to analyze the impact of different module designs on the model performance. We set $k = 1$ in k-degree overlapping fragmentation for fair comparison. We define the *normalized performance* as the RMSE divided by the standard deviation of the labels for regression tasks. For classification tasks, it is calcuated by $1 - \text{AUROC}$. A lower normalized value indicates better performance.

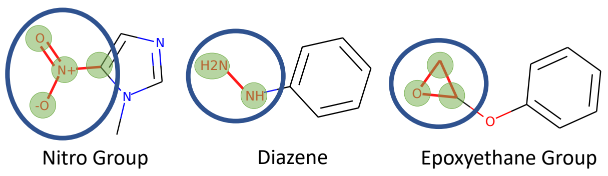

Figure 4: Interpretation results of FragCAM on mutagenicity datasets. The green nodes are the ground truth alerts. The blue fragments are the fragments with the highest attribution score in FragCAM.

Table 4: Performance comparison between FragCAM and SubgraphX on DrugXAI. The best results are in bold. N_{min} represents the target number of fragment nodes in SubgraphX.

	SubgraphX				FragCAM
N_{min}	3	7	10	15	–
AUROC	0.655	0.683	0.663	0.592	**0.793**
Fidelity(sparsity)	0.24(0.81)	0.29(0.58)	0.30(0.41)	0.28(0.21)	**0.35(0.72)**
Time per sample (s)	52	28	17	11	**0.024**

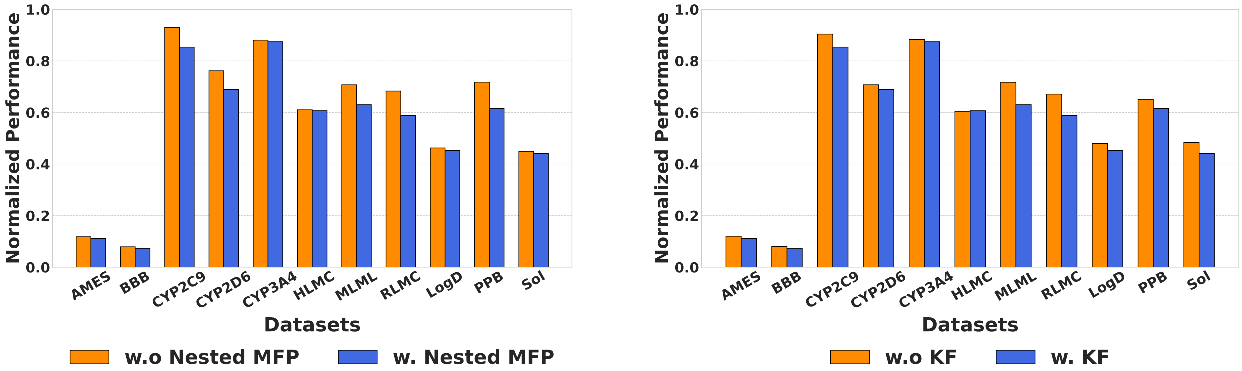

Figure 5: Left: Comparison between nested masked fragment prediction (w.) and cross entropy loss (w.o). "MFP": masked fragment prediction. Right: Comparison between models w./w.o knowledge fusion (KF).

Table 6: Comparison between different mask rates in pre-training.

	Classfication (AUROC ↑)		Regression (RMSE ↓)									Average Rank
Mask Rate	AMES	BBB	CYP2C9	CYP2D6	CYP3A4	HLMC	MLMC	RLMC	LogD	PPB	Sol	
0.1	0.879	0.924	17.886	16.676	16.298	0.523	0.733	**0.592**	0.698	0.174	0.922	2.2
0.3	**0.889**	**0.927**	**16.855**	**14.425**	**15.894**	**0.514**	**0.702**	0.596	**0.667**	**0.157**	**0.895**	1.1
0.5	0.868	0.919	17.527	16.627	16.379	0.527	0.738	0.621	0.689	0.180	0.924	2.7

Effectiveness of Nested Masked Fragment Predictions To evaluate the effect of the nested masked fragment prediction criterion, we pre-train the model with cross entropy loss which only predicts the identity of the masked fragment. The finetuning procedure remains unchanged. The results are illustrated in Figure 5 (left). We can see that the nested masked fragment prediction consistently outperforms the cross-entropy loss, often by a substantial margin, particularly for CYP2C9, CYP2D6, MLMC, RLMC, and PPB datasets.

Impact of Knowledge Fusion Layer We compare models with and without knowledge fusion layer. The results, displayed in Figure 5 (right), reveal that the model utilizing knowledge fusion layer outperforms its counterpart on most datasets except for HLMC, demonstrating the efficacy of our knowledge fusion module.

How Vocabulary Size Affects Performance? To evaluate the influence of vocabulary size, we vary the fragment vocabulary size to 200, 500, and 1000. The results are presented in Table 5. Notably, each vocabulary size achieves the best performance on at least one dataset. On average, a vocabulary size of 500 yields the best overall performance w.r.t average rank. If the vocabulary size is too small, it may not be able to capture the diversity of fragments, whereas an overly large vocabulary can introduce redundant fragments.

Effect of Mask Rate in Pre-training We investigate the effect of the mask rate in pre-training by adjusting it to 0.1, 0.3, and 0.5. The results, shown in Table 6, indicate that a mask rate of 0.3 provides the best performance across nearly all datasets. A mask rate that is too high can make the pre-training task too

Table 5: Comparison between different fragment vocabulary sizes.

	Classfication (AUROC ↑)		Regression (RMSE ↓)									Average Rank
Vocab Size	AMES	BBB	CYP2C9	CYP2D6	CYP3A4	HLMC	MLMC	RLMC	LogD	PPB	Sol	
200	0.855	0.923	17.177	15.033	15.960	**0.508**	0.705	0.610	0.670	0.171	0.910	2.7
500	**0.889**	**0.927**	16.855	**14.425**	15.894	0.514	0.702	0.596	**0.667**	**0.157**	**0.895**	1.3
1000	0.878	0.922	**16.678**	15.234	**15.697**	0.535	**0.675**	**0.549**	0.679	0.170	0.897	2.0

hard for the model to learn, while one that is too low may make the pre-training process excessively easy, offering little benefit for developing useful fragment representations.

5 Conclusion

In this paper, we propose a self-supervised learning framework, *FragFormer*, designed for molecular property prediction that enhances both performance and model interpretability. FragFormer features a novel molecule fragmentation method *DOVE* which generates overlapping fragments through iterative line graph transformation. Additionally, we implement a *nested masked fragment prediction* task to help the model learn the hierarchical fragment representations, along with a knowledge fusion layer to integrate fixed molecular features. To facilitate interpretability, we propose a simple yet effective method called *FragCAM*, which identifies the critical fragments contributing to predictions. FragFormer achieves state-of-the-art performance on eight out of eleven molecular property prediction tasks on PharmaBench and surpasses strong baseline models on long-range biological benchmark. Furthermore, FragFormer demonstrates superior interpretability on both synthetic and real-world molecular datasets, effectively identifying decisive fragments.

Acknowledgments

This work was supported by Beijing Natural Science Foundation NO. 4252046.

References

Abien Fred Agarap. Deep learning using rectified linear units (relu). *CoRR*, abs/1803.08375, 2018. URL http://arxiv.org/abs/1803.08375.

Bruce N. Ames, Frank Lee, and William Durston. An improved bacterial test system for the detection and classification of mutagens and carcinogens. *Proceedings of the National Academy of Sciences of the United States of America*, 70 3:782–6, 1973. URL https://api.semanticscholar.org/CorpusID:29499607.

Alexei Baevski, Yuhao Zhou, Abdelrahman Mohamed, and Michael Auli. wav2vec 2.0: A framework for self-supervised learning of speech representations. In Hugo Larochelle, Marc'Aurelio Ranzato, Raia Hadsell, Maria-Florina Balcan, and Hsuan-Tien Lin (eds.), *Advances in Neural Information Processing Systems 33: Annual Conference on Neural Information Processing Systems 2020, NeurIPS 2020, December 6-12, 2020, virtual*, 2020. URL https://proceedings.neurips.cc/paper/2020/hash/92d1e1eb1cd6f9fba3227870bb6d7f07-Abstract.html.

Viraj Bagal, Rishal Aggarwal, P. K. Vinod, and U. Deva Priyakumar. Molgpt: Molecular generation using a transformer-decoder model. *J. Chem. Inf. Model.*, 62(9):2064–2076, 2022. doi: 10.1021/ACS.JCIM.1C00600. URL https://doi.org/10.1021/acs.jcim.1c00600.

Peter W. Battaglia, Jessica B. Hamrick, Victor Bapst, Alvaro Sanchez-Gonzalez, Vinícius Flores Zambaldi, Mateusz Malinowski, Andrea Tacchetti, David Raposo, Adam Santoro, Ryan Faulkner, Çaglar Gülçehre, H. Francis Song, Andrew J. Ballard, Justin Gilmer, George E. Dahl, Ashish Vaswani, Kelsey R. Allen, Charles Nash, Victoria Langston, Chris Dyer, Nicolas Heess, Daan Wierstra, Pushmeet Kohli, Matthew M. Botvinick, Oriol Vinyals, Yujia Li, and Razvan Pascanu. Relational inductive biases, deep learning, and graph networks. *CoRR*, abs/1806.01261, 2018. URL http://arxiv.org/abs/1806.01261.

Giorgos Bouritsas, Fabrizio Frasca, Stefanos Zafeiriou, and Michael M. Bronstein. Improving graph neural network expressivity via subgraph isomorphism counting. *IEEE Trans. Pattern Anal. Mach. Intell.*, 45 (1):657–668, 2023. doi: 10.1109/TPAMI.2022.3154319. URL `https://doi.org/10.1109/TPAMI.2022.3154319`.

Leo Breiman. Random forests. *Mach. Learn.*, 45(1):5–32, 2001. doi: 10.1023/A:1010933404324. URL `https://doi.org/10.1023/A:1010933404324`.

Xavier Bresson and Thomas Laurent. Residual gated graph convnets. *CoRR*, abs/1711.07553, 2017. URL `http://arxiv.org/abs/1711.07553`.

Hanxuan Cai, Huimin Zhang, Duancheng Zhao, Jingxing Wu, and Ling Wang. FP-GNN: a versatile deep learning architecture for enhanced molecular property prediction. *Briefings Bioinform.*, 23(6), 2022. doi: 10.1093/BIB/BBAC408. URL `https://doi.org/10.1093/bib/bbac408`.

Baiyu Chen, Ziqi Pan, Minjie Mou, Yuan Zhou, and Wei Fu. Is fragment-based graph a better graph-based molecular representation for drug design? a comparison study of graph-based models. *Comput. Biol. Med.*, 169(C), April 2024. ISSN 0010-4825. doi: 10.1016/j.compbiomed.2023.107811. URL `https://doi.org/10.1016/j.compbiomed.2023.107811`.

Hongming Chen, Ola Engkvist, Yinhai Wang, Marcus Olivecrona, and Thomas Blaschke. The rise of deep learning in drug discovery. *Drug discovery today*, 23 6:1241–1250, 2018. URL `https://api.semanticscholar.org/CorpusID:46792472`.

Ming Chen, Zhewei Wei, Zengfeng Huang, Bolin Ding, and Yaliang Li. Simple and deep graph convolutional networks. In *Proceedings of the 37th International Conference on Machine Learning, ICML 2020, 13-18 July 2020, Virtual Event*, volume 119 of *Proceedings of Machine Learning Research*, pp. 1725–1735. PMLR, 2020a. URL `http://proceedings.mlr.press/v119/chen20v.html`.

Tianqi Chen and Carlos Guestrin. Xgboost: A scalable tree boosting system. In Balaji Krishnapuram, Mohak Shah, Alexander J. Smola, Charu Aggarwal, Dou Shen, and Rajeev Rastogi (eds.), *KDD*, pp. 785–794. ACM, 2016. ISBN 978-1-4503-4232-2. URL `http://dblp.uni-trier.de/db/conf/kdd/kdd2016.html#ChenG16`.

Ting Chen, Simon Kornblith, Mohammad Norouzi, and Geoffrey E. Hinton. A simple framework for contrastive learning of visual representations. In *Proceedings of the 37th International Conference on Machine Learning, ICML 2020, 13-18 July 2020, Virtual Event*, volume 119 of *Proceedings of Machine Learning Research*, pp. 1597–1607. PMLR, 2020b. URL `http://proceedings.mlr.press/v119/chen20j.html`.

Corinna Cortes and Vladimir Vapnik. Support-vector networks. *Mach. Learn.*, 20(3):273–297, 1995. doi: 10.1007/BF00994018. URL `https://doi.org/10.1007/BF00994018`.

Jörg Degen, Christof Wegscheid-Gerlach, Andrea Zaliani, and Matthias Rarey. On the art of compiling and using 'drug-like' chemical fragment spaces. *ChemMedChem*, 3(10):1503–1507, 2008. ISSN 1860-7187. doi: 10.1002/cmdc.200800178.

Jacob Devlin, Ming-Wei Chang, Kenton Lee, and Kristina Toutanova. BERT: pre-training of deep bidirectional transformers for language understanding. In Jill Burstein, Christy Doran, and Thamar Solorio (eds.), *Proceedings of the 2019 Conference of the North American Chapter of the Association for Computational Linguistics: Human Language Technologies, NAACL-HLT 2019, Minneapolis, MN, USA, June 2-7, 2019, Volume 1 (Long and Short Papers)*, pp. 4171–4186. Association for Computational Linguistics, 2019. doi: 10.18653/V1/N19-1423. URL `https://doi.org/10.18653/v1/n19-1423`.

Michael Dickson and Jean Paul Gagnon. Key factors in the rising cost of new drug discovery and development. *Nature Reviews Drug Discovery*, 3:417–429, 2004. URL `https://api.semanticscholar.org/CorpusID:28009388`.

Joseph L. Durant, Burton A. Leland, Douglas R. Henry, and James G. Nourse. Reoptimization of mdl keys for use in drug discovery. *Journal of chemical information and computer sciences*, 42 6:1273–80, 2002. URL `https://api.semanticscholar.org/CorpusID:22752474`.

Vijay Prakash Dwivedi, Chaitanya K. Joshi, Thomas Laurent, Yoshua Bengio, and Xavier Bresson. Benchmarking graph neural networks. *CoRR*, abs/2003.00982, 2020. URL https://arxiv.org/abs/2003.00982.

Vijay Prakash Dwivedi, Anh Tuan Luu, Thomas Laurent, Yoshua Bengio, and Xavier Bresson. Graph neural networks with learnable structural and positional representations. In *The Tenth International Conference on Learning Representations, ICLR 2022, Virtual Event, April 25-29, 2022*. OpenReview.net, 2022a. URL https://openreview.net/forum?id=wTTjnvGphYj.

Vijay Prakash Dwivedi, Ladislav Rampásek, Michael Galkin, Ali Parviz, Guy Wolf, Anh Tuan Luu, and Dominique Beaini. Long range graph benchmark. In Sanmi Koyejo, S. Mohamed, A. Agarwal, Danielle Belgrave, K. Cho, and A. Oh (eds.), *Advances in Neural Information Processing Systems 35: Annual Conference on Neural Information Processing Systems 2022, NeurIPS 2022, New Orleans, LA, USA, November 28 - December 9, 2022*, 2022b. URL http://papers.nips.cc/paper_files/paper/2022/hash/8c3c666820ea055a77726d66fc7d447f-Abstract-Datasets_and_Benchmarks.html.

Benedek Fabian, Thomas Edlich, Héléna Gaspar, Marwin H. S. Segler, Joshua Meyers, Marco Fiscato, and Mohamed Ahmed. Molecular representation learning with language models and domain-relevant auxiliary tasks. *CoRR*, abs/2011.13230, 2020. URL https://arxiv.org/abs/2011.13230.

Xiaomin Fang, Lihang Liu, Jieqiong Lei, Donglong He, Shanzhuo Zhang, Jingbo Zhou, Fan Wang, Hua Wu, and Haifeng Wang. Geometry-enhanced molecular representation learning for property prediction. *Nature Machine Intelligence*, 4:127 – 134, 2021. URL https://api.semanticscholar.org/CorpusID:235417265.

Yin Fang, Qiang Zhang, Ningyu Zhang, Zhuo Chen, Xiang Zhuang, Xin Shao, Xiaohui Fan, and Huajun Chen. Knowledge graph-enhanced molecular contrastive learning with functional prompt. *Nat. Mac. Intell.*, 5(5): 542–553, 2023. doi: 10.1038/S42256-023-00654-0. URL https://doi.org/10.1038/s42256-023-00654-0.

Anna Gaulton, Anne Hersey, Michał Nowotka, A. Patrícia Bento, Jon Chambers, David Mendez, Prudence Mutowo, Francis Atkinson, Louisa J. Bellis, Elena Cibrián-Uhalte, Mark Davies, Nathan Dedman, Anneli Karlsson, María Paula Magariños, John P. Overington, George Papadatos, Ines Smit, and Andrew R. Leach. The chembl database in 2017. *Nucleic Acids Research*, pp. D945–D954, Jan 2017. doi: 10.1093/nar/gkw1074. URL http://dx.doi.org/10.1093/nar/gkw1074.

Zhichun Guo, Chuxu Zhang, Wenhao Yu, John Herr, Olaf Wiest, Meng Jiang, and Nitesh V. Chawla. Few-shot graph learning for molecular property prediction. In Jure Leskovec, Marko Grobelnik, Marc Najork, Jie Tang, and Leila Zia (eds.), *WWW '21: The Web Conference 2021, Virtual Event / Ljubljana, Slovenia, April 19-23, 2021*, pp. 2559–2567. ACM / IW3C2, 2021. doi: 10.1145/3442381.3450112. URL https://doi.org/10.1145/3442381.3450112.

Olgun Guvench. Computational functional group mapping for drug discovery. *Drug discovery today*, 21 12: 1928–1931, 2016. URL https://api.semanticscholar.org/CorpusID:39937186.

William L. Hamilton, Zhitao Ying, and Jure Leskovec. Inductive representation learning on large graphs. In Isabelle Guyon, Ulrike von Luxburg, Samy Bengio, Hanna M. Wallach, Rob Fergus, S. V. N. Vishwanathan, and Roman Garnett (eds.), *Advances in Neural Information Processing Systems 30: Annual Conference on Neural Information Processing Systems 2017, December 4-9, 2017, Long Beach, CA, USA*, pp. 1024–1034, 2017a. URL https://proceedings.neurips.cc/paper/2017/hash/5dd9db5e033da9c6fb5ba83c7a7ebea9-Abstract.html.

William L. Hamilton, Zhitao Ying, and Jure Leskovec. Inductive representation learning on large graphs. In Isabelle Guyon, Ulrike von Luxburg, Samy Bengio, Hanna M. Wallach, Rob Fergus, S. V. N. Vishwanathan, and Roman Garnett (eds.), *Advances in Neural Information Processing Systems 30: Annual Conference on Neural Information Processing Systems 2017, December 4-9, 2017, Long Beach, CA, USA*, pp. 1024–1034, 2017b. URL https://proceedings.neurips.cc/paper/2017/hash/5dd9db5e033da9c6fb5ba83c7a7ebea9-Abstract.html.

Corwin Hansch, Peyton P. Maloney, Toshio Fujita, and Robert M. Muir. Correlation of biological activity of phenoxyacetic acids with hammett substituent constants and partition coefficients. *Nature*, 194:178–180, 1962. URL https://api.semanticscholar.org/CorpusID:4189723.

Kaiming He, Xinlei Chen, Saining Xie, Yanghao Li, Piotr Dollár, and Ross B. Girshick. Masked autoencoders are scalable vision learners. In *IEEE/CVF Conference on Computer Vision and Pattern Recognition, CVPR 2022, New Orleans, LA, USA, June 18-24, 2022*, pp. 15979–15988. IEEE, 2022. doi: 10.1109/CVPR52688.2022.01553. URL `https://doi.org/10.1109/CVPR52688.2022.01553`.

Zhenyu Hou, Xiao Liu, Yukuo Cen, Yuxiao Dong, Hongxia Yang, Chunjie Wang, and Jie Tang. Graphmae: Self-supervised masked graph autoencoders. In Aidong Zhang and Huzefa Rangwala (eds.), *KDD '22: The 28th ACM SIGKDD Conference on Knowledge Discovery and Data Mining, Washington, DC, USA, August 14 - 18, 2022*, pp. 594–604. ACM, 2022. doi: 10.1145/3534678.3539321. URL `https://doi.org/10.1145/3534678.3539321`.

Wei-Ning Hsu, Benjamin Bolte, Yao-Hung Hubert Tsai, Kushal Lakhotia, Ruslan Salakhutdinov, and Abdelrahman Mohamed. Hubert: Self-supervised speech representation learning by masked prediction of hidden units. *IEEE ACM Trans. Audio Speech Lang. Process.*, 29:3451–3460, 2021. doi: 10.1109/TASLP.2021.3122291. URL `https://doi.org/10.1109/TASLP.2021.3122291`.

Weihua Hu, Bowen Liu, Joseph Gomes, Marinka Zitnik, Percy Liang, Vijay S. Pande, and Jure Leskovec. Strategies for pre-training graph neural networks. In *8th International Conference on Learning Representations, ICLR 2020, Addis Ababa, Ethiopia, April 26-30, 2020*. OpenReview.net, 2020. URL `https://openreview.net/forum?id=HJlWWJSFDH`.

Yinghui Jiang, Shuting Jin, Xurui Jin, Xianglu Xiao, Wenfan Wu, Xiangrong Liu, Qian Zhang, Xiangxiang Zeng, Guang Yang, and Zhangming Niu. Pharmacophoric-constrained heterogeneous graph transformer model for molecular property prediction. *Communications Chemistry*, 6, 2023. URL `https://api.semanticscholar.org/CorpusID:257903087`.

Wengong Jin, Regina Barzilay, and Tommi S. Jaakkola. Junction tree variational autoencoder for molecular graph generation. In Jennifer G. Dy and Andreas Krause (eds.), *Proceedings of the 35th International Conference on Machine Learning, ICML 2018, Stockholmsmässan, Stockholm, Sweden, July 10-15, 2018*, volume 80 of *Proceedings of Machine Learning Research*, pp. 2328–2337. PMLR, 2018. URL `http://proceedings.mlr.press/v80/jin18a.html`.

Wengong Jin, Regina Barzilay, and Tommi S. Jaakkola. Hierarchical generation of molecular graphs using structural motifs. In *Proceedings of the 37th International Conference on Machine Learning, ICML 2020, 13-18 July 2020, Virtual Event*, volume 119 of *Proceedings of Machine Learning Research*, pp. 4839–4848. PMLR, 2020. URL `http://proceedings.mlr.press/v119/jin20a.html`.

Seojin Kim, Jaehyun Nam, Junsu Kim, Hankook Lee, Sungsoo Ahn, and Jinwoo Shin. Holistic molecular representation learning via multi-view fragmentation. *Trans. Mach. Learn. Res.*, 2024, 2024. URL `https://openreview.net/forum?id=ufDh55J1ML`.

Sunghwan Kim, Jie Chen, Tiejun Cheng, Asta Gindulyte, Jia He, Siqian He, Qingliang Li, Benjamin A. Shoemaker, Paul A. Thiessen, Bo Yu, Leonid Y. Zaslavsky, Jian Zhang, and Evan E. Bolton. Pubchem 2023 update. *Nucleic acids research*, 2022. URL `https://api.semanticscholar.org/CorpusID:253182955`.

Diederik P. Kingma and Jimmy Ba. Adam: A method for stochastic optimization. In Yoshua Bengio and Yann LeCun (eds.), *3rd International Conference on Learning Representations, ICLR 2015, San Diego, CA, USA, May 7-9, 2015, Conference Track Proceedings*, 2015. URL `http://arxiv.org/abs/1412.6980`.

Diederik P. Kingma and Max Welling. Auto-encoding variational bayes. In Yoshua Bengio and Yann LeCun (eds.), *2nd International Conference on Learning Representations, ICLR 2014, Banff, AB, Canada, April 14-16, 2014, Conference Track Proceedings*, 2014. URL `http://arxiv.org/abs/1312.6114`.

Thomas N. Kipf and Max Welling. Semi-supervised classification with graph convolutional networks. In *5th International Conference on Learning Representations, ICLR 2017, Toulon, France, April 24-26, 2017, Conference Track Proceedings*. OpenReview.net, 2017. URL `https://openreview.net/forum?id=SJU4ayYgl`.

Narine Kokhlikyan, Vivek Miglani, Miguel Martin, Edward Wang, Bilal Alsallakh, Jonathan Reynolds, Alexander Melnikov, Natalia Kliushkina, Carlos Araya, Siqi Yan, and Orion Reblitz-Richardson. Captum: A unified and generic model interpretability library for pytorch. *CoRR*, abs/2009.07896, 2020. URL `https://arxiv.org/abs/2009.07896`.

Xiangzhe Kong, Wenbing Huang, Zhixing Tan, and Yang Liu. Molecule generation by principal subgraph mining and assembling. In Sanmi Koyejo, S. Mohamed, A. Agarwal, Danielle Belgrave, K. Cho, and A. Oh (eds.), *Advances in Neural Information Processing Systems 35: Annual Conference on Neural Information Processing Systems 2022, NeurIPS 2022, New Orleans, LA, USA, November 28 - December 9, 2022*, 2022. URL `http://papers.nips.cc/paper_files/paper/2022/hash/1160792eab11de2bbaf9e71fce191e8c-Abstract-Conference.html`.

Devin Kreuzer, Dominique Beaini, William L. Hamilton, Vincent Létourneau, and Prudencio Tossou. Rethinking graph transformers with spectral attention. In Marc'Aurelio Ranzato, Alina Beygelzimer, Yann N. Dauphin, Percy Liang, and Jennifer Wortman Vaughan (eds.), *Advances in Neural Information Processing Systems 34: Annual Conference on Neural Information Processing Systems 2021, NeurIPS 2021, December 6-14, 2021, virtual*, pp. 21618–21629, 2021. URL `https://proceedings.neurips.cc/paper/2021/hash/b4fd1d2cb085390fbbadae65e07876a7-Abstract.html`.

Greg Landrum. Rdkit: Open-source cheminformatics software. 2016. URL `https://github.com/rdkit/rdkit/releases/tag/Release_2016_09_4`.

Xiao Qing Lewell, Duncan B. Judd, Stephen P. Watson, and Michael M. Hann. Recapretrosynthetic combinatorial analysis procedure: A powerful new technique for identifying privileged molecular fragments with useful applications in combinatorial chemistry. *Journal of Chemical Information and Computer Sciences*, 38(3):511–522, May 1998. doi: 10.1021/ci970429i.

Han Li, Ruotian Zhang, Min Yaosen, Dacheng Ma, Dan Zhao, and Jianyang Zeng. A knowledge-guided pre-training framework for improving molecular representation learning. *Nature Communications*, 14, 11 2023. doi: 10.1038/s41467-023-43214-1.

Pengyong Li, Jun Wang, Yixuan Qiao, Hao Chen, Yihuan Yu, Xiaojun Yao, Peng Gao, Guotong Xie, and Sen Song. An effective self-supervised framework for learning expressive molecular global representations to drug discovery. *Briefings Bioinform.*, 22(6), 2021. doi: 10.1093/BIB/BBAB109. URL `https://doi.org/10.1093/bib/bbab109`.

Shengchao Liu, Hanchen Wang, Weiyang Liu, Joan Lasenby, Hongyu Guo, and Jian Tang. Pre-training molecular graph representation with 3d geometry. In *The Tenth International Conference on Learning Representations, ICLR 2022, Virtual Event, April 25-29, 2022*. OpenReview.net, 2022. URL `https://openreview.net/forum?id=xQUe1pOKPam`.

Shengchao Liu, Weili Nie, Chengpeng Wang, Jiarui Lu, Zhuoran Qiao, Ling Liu, Jian Tang, Chaowei Xiao, and Anima Anandkumar. Multi-modal molecule structure-text model for text-based retrieval and editing. *Nature Machine Intelligence*, 5(12):1447–1457, Dec 2023. ISSN 2522-5839. doi: 10.1038/s42256-023-00759-6. URL `https://doi.org/10.1038/s42256-023-00759-6`.

Dongsheng Luo, Wei Cheng, Dongkuan Xu, Wenchao Yu, Bo Zong, Haifeng Chen, and Xiang Zhang. Parameterized explainer for graph neural network. In Hugo Larochelle, Marc'Aurelio Ranzato, Raia Hadsell, Maria-Florina Balcan, and Hsuan-Tien Lin (eds.), *Advances in Neural Information Processing Systems 33: Annual Conference on Neural Information Processing Systems 2020, NeurIPS 2020, December 6-12, 2020, virtual*, 2020. URL `https://proceedings.neurips.cc/paper/2020/hash/e37b08dd3015330dcbb5d6663667b8b8-Abstract.html`.

Shengjie Luo, Tianlang Chen, Yixian Xu, Shuxin Zheng, Tie-Yan Liu, Liwei Wang, and Di He. One transformer can understand both 2d & 3d molecular data. In *The Eleventh International Conference on Learning Representations, ICLR 2023, Kigali, Rwanda, May 1-5, 2023*. OpenReview.net, 2023. URL `https://openreview.net/forum?id=vZTp1oPV3PC`.

Kha-Dinh Luong and Ambuj K. Singh. Fragment-based pretraining and finetuning on molecular graphs. In Alice Oh, Tristan Naumann, Amir Globerson, Kate Saenko, Moritz Hardt, and Sergey Levine (eds.), *Advances in Neural Information Processing Systems 36: Annual Conference on Neural Information Processing Systems 2023, NeurIPS 2023, New Orleans, LA, USA, December 10 - 16, 2023*, 2023. URL `http://papers.nips.cc/paper_files/paper/2023/hash/38ec60a949c3538e5cbb337b1b386dcf-Abstract-Conference.html`.

Ricardo Macarron, Martyn N. Banks, Dejan Bojanic, David J. Burns, Dragan A. Cirovic, Tina Garyantes, Darren V. S. Green, Robert P. Hertzberg, William P. Janzen, Jeff W. Paslay, Ulrich Schopfer, and G. Sittampalam. Impact of high-throughput screening in biomedical research. *Nature Reviews Drug Discovery*, 10:188–195, 2011. URL `https://api.semanticscholar.org/CorpusID:205477370`.

Dominic Masters, Josef Dean, Kerstin Kläser, Zhiyi Li, Samuel Maddrell-Mander, Adam Sanders, Hatem Helal, Deniz Beker, Andrew W. Fitzgibbon, Shenyang Huang, Ladislav Rampásek, and Dominique Beaini. GPS++: reviving the art of message passing for molecular property prediction. *Trans. Mach. Learn. Res.*, 2023, 2023. URL `https://openreview.net/forum?id=moVEUgJaHO`.

Kevin McCloskey, Ankur Taly, Federico Monti, Michael P. Brenner, and Lucy J. Colwell. Using attribution to decode binding mechanism in neural network models for chemistry. *Proceedings of the National Academy of Sciences*, 116(24):11624–11629, Jun 2019. doi: 10.1073/pnas.1820657116. URL `http://dx.doi.org/10.1073/pnas.1820657116`.

Cédric Merlot, Daniel Domine, Christophe Cleva, and Dennis J Church. Chemical substructures in drug discovery. *Drug discovery today*, 8 13:594–602, 2003. URL `https://api.semanticscholar.org/CorpusID:35874487`.

Asher Mullard. New drugs cost us$2.6 billion to develop. *Nature Reviews Drug Discovery*, 13:877–877, 2014. URL `https://api.semanticscholar.org/CorpusID:12198576`.

Christopher W. Murray and David C Rees. The rise of fragment-based drug discovery. *Nature chemistry*, 1 3: 187–92, 2009. URL `https://api.semanticscholar.org/CorpusID:24739755`.

Zhangming Niu, Xianglu Xiao, Wenfan Wu, Qiwei Cai, Yinghui Jiang, Wangzhen Jin, Minhao Wang, Guojian Yang, Lingkang Kong, Xurui Jin, Guan Yang, and Hongming Chen. Pharmabench: Enhancing admet benchmarks with large language models. *Scientific Data*, 11, 2024. URL `https://api.semanticscholar.org/CorpusID:272553326`.

Adam Paszke, Sam Gross, Francisco Massa, Adam Lerer, James Bradbury, Gregory Chanan, Trevor Killeen, Zeming Lin, Natalia Gimelshein, Luca Antiga, Alban Desmaison, Andreas Köpf, Edward Z. Yang, Zachary DeVito, Martin Raison, Alykhan Tejani, Sasank Chilamkurthy, Benoit Steiner, Lu Fang, Junjie Bai, and Soumith Chintala. Pytorch: An imperative style, high-performance deep learning library. In Hanna M. Wallach, Hugo Larochelle, Alina Beygelzimer, Florence d'Alché-Buc, Emily B. Fox, and Roman Garnett (eds.), *Advances in Neural Information Processing Systems 32: Annual Conference on Neural Information Processing Systems 2019, NeurIPS 2019, December 8-14, 2019, Vancouver, BC, Canada*, pp. 8024–8035, 2019. URL `https://proceedings.neurips.cc/paper/2019/hash/bdbca288fee7f92f2bfa9f7012727740-Abstract.html`.

Phillip E. Pope, Soheil Kolouri, Mohammad Rostami, Charles E. Martin, and Heiko Hoffmann. Explainability methods for graph convolutional neural networks. In *IEEE Conference on Computer Vision and Pattern Recognition, CVPR 2019, Long Beach, CA, USA, June 16-20, 2019*, pp. 10772–10781. Computer Vision Foundation / IEEE, 2019. doi: 10.1109/CVPR.2019.01103. URL `http://openaccess.thecvf.com/content_CVPR_2019/html/Pope_Explainability_Methods_for_Graph_Convolutional_Neural_Networks_CVPR_2019_paper.html`.

Michela Proietti, Alessio Ragno, Biagio La Rosa, Rino Ragno, and Roberto Capobianco. Explainable AI in drug discovery: self-interpretable graph neural network for molecular property prediction using concept whitening. *Mach. Learn.*, 113(4):2013–2044, 2024. doi: 10.1007/S10994-023-06369-Y. URL `https://doi.org/10.1007/s10994-023-06369-y`.

Jiahua Rao, Shuangjia Zheng, and Yuedong Yang. Quantitative evaluation of explainable graph neural networks for molecular property prediction. *CoRR*, abs/2107.04119, 2021. URL https://arxiv.org/abs/2107.04119.

Matthias Rarey and J. Scott Dixon. Feature trees: A new molecular similarity measure based on tree matching. *J. Comput. Aided Mol. Des.*, 12(5):471–490, 1998. doi: 10.1023/A:1008068904628. URL https://doi.org/10.1023/A:1008068904628.

David Rogers and Mathew Hahn. Extended-connectivity fingerprints. *J. Chem. Inf. Model.*, 50(5):742–754, 2010. doi: 10.1021/CI100050T. URL https://doi.org/10.1021/ci100050t.

Yu Rong, Yatao Bian, Tingyang Xu, Weiyang Xie, Ying Wei, Wenbing Huang, and Junzhou Huang. Self-supervised graph transformer on large-scale molecular data. In Hugo Larochelle, Marc'Aurelio Ranzato, Raia Hadsell, Maria-Florina Balcan, and Hsuan-Tien Lin (eds.), *Advances in Neural Information Processing Systems 33: Annual Conference on Neural Information Processing Systems 2020, NeurIPS 2020, December 6-12, 2020, virtual*, 2020. URL https://proceedings.neurips.cc/paper/2020/hash/94aef38441efa3380a3bed3faf1f9d5d-Abstract.html.

Jerret Ross, Brian M. Belgodere, Vijil Chenthamarakshan, Inkit Padhi, Youssef Mroueh, and Payel Das. Large-scale chemical language representations capture molecular structure and properties. *Nature Machine Intelligence*, 4:1256–1264, 2021. URL https://api.semanticscholar.org/CorpusID:254636625.

T. Konstantin Rusch, Michael M. Bronstein, and Siddhartha Mishra. A survey on oversmoothing in graph neural networks. *CoRR*, abs/2303.10993, 2023. doi: 10.48550/ARXIV.2303.10993. URL https://doi.org/10.48550/arXiv.2303.10993.

Tanja Schulz-Gasch, Christin Schärfer, Wolfgang Guba, and Matthias Rarey. TFD: torsion fingerprints as a new measure to compare small molecule conformations. *J. Chem. Inf. Model.*, 52(6):1499–1512, 2012. doi: 10.1021/CI2002318. URL https://doi.org/10.1021/ci2002318.

Ramprasaath R. Selvaraju, Michael Cogswell, Abhishek Das, Ramakrishna Vedantam, Devi Parikh, and Dhruv Batra. Grad-cam: Visual explanations from deep networks via gradient-based localization. *Int. J. Comput. Vis.*, 128(2):336–359, 2020. doi: 10.1007/S11263-019-01228-7. URL https://doi.org/10.1007/s11263-019-01228-7.

Rico Sennrich, Barry Haddow, and Alexandra Birch. Neural machine translation of rare words with subword units. In *Proceedings of the 54th Annual Meeting of the Association for Computational Linguistics, ACL 2016, August 7-12, 2016, Berlin, Germany, Volume 1: Long Papers*. The Association for Computer Linguistics, 2016. doi: 10.18653/V1/P16-1162. URL https://doi.org/10.18653/v1/p16-1162.

Yu Shi, Shuxin Zheng, Guolin Ke, Yifei Shen, Jiacheng You, Jiyan He, Shengjie Luo, Chang Liu, Di He, and Tie-Yan Liu. Benchmarking graphormer on large-scale molecular modeling datasets. *CoRR*, abs/2203.04810, 2022. doi: 10.48550/ARXIV.2203.04810. URL https://doi.org/10.48550/arXiv.2203.04810.

Avanti Shrikumar, Peyton Greenside, and Anshul Kundaje. Learning important features through propagating activation differences. In Doina Precup and Yee Whye Teh (eds.), *Proceedings of the 34th International Conference on Machine Learning, ICML 2017, Sydney, NSW, Australia, 6-11 August 2017*, volume 70 of *Proceedings of Machine Learning Research*, pp. 3145–3153. PMLR, 2017. URL http://proceedings.mlr.press/v70/shrikumar17a.html.

Steven R A Simoens and Isabelle Huys. R&d costs of new medicines: A landscape analysis. *Frontiers in Medicine*, 8, 2021. URL https://api.semanticscholar.org/CorpusID:239770727.

Ying Song, Shuangjia Zheng, Zhangming Niu, Zhang-Hua Fu, Yutong Lu, and Yuedong Yang. Communicative representation learning on attributed molecular graphs. In Christian Bessiere (ed.), *Proceedings of the Twenty-Ninth International Joint Conference on Artificial Intelligence, IJCAI 2020*, pp. 2831–2838. ijcai.org, 2020. doi: 10.24963/IJCAI.2020/392. URL https://doi.org/10.24963/ijcai.2020/392.

Yuanbing Song, Jinghua Chen, Wenju Wang, Gang Chen, and Zhichong Ma. Double-head transformer neural network for molecular property prediction. *J. Cheminformatics*, 15(1):27, 2023. doi: 10.1186/S13321-023-00700-4. URL https://doi.org/10.1186/s13321-023-00700-4.

Hannes Stärk, Dominique Beaini, Gabriele Corso, Prudencio Tossou, Christian Dallago, Stephan Günnemann, and Pietro Lió. 3d infomax improves gnns for molecular property prediction. In Kamalika Chaudhuri, Stefanie Jegelka, Le Song, Csaba Szepesvári, Gang Niu, and Sivan Sabato (eds.), *International Conference on Machine Learning, ICML 2022, 17-23 July 2022, Baltimore, Maryland, USA*, volume 162 of *Proceedings of Machine Learning Research*, pp. 20479–20502. PMLR, 2022. URL https://proceedings.mlr.press/v162/stark22a.html.

Teague Sterling and John J. Irwin. ZINC 15 - ligand discovery for everyone. *J. Chem. Inf. Model.*, 55(11): 2324–2337, 2015. doi: 10.1021/ACS.JCIM.5B00559. URL https://doi.org/10.1021/acs.jcim.5b00559.

Mukund Sundararajan, Ankur Taly, and Qiqi Yan. Axiomatic attribution for deep networks. In Doina Precup and Yee Whye Teh (eds.), *Proceedings of the 34th International Conference on Machine Learning, ICML 2017, Sydney, NSW, Australia, 6-11 August 2017*, volume 70 of *Proceedings of Machine Learning Research*, pp. 3319–3328. PMLR, 2017. URL http://proceedings.mlr.press/v70/sundararajan17a.html.

Iurii Sushko, Elena Salmina, Vladimir Potemkin, Gennadiy Poda, and Igor V. Tetko. Toxalerts: A web server of structural alerts for toxic chemicals and compounds with potential adverse reactions. *J. Chem. Inf. Model.*, 52(8):2310–2316, 2012. doi: 10.1021/CI300245Q. URL https://doi.org/10.1021/ci300245q.

Alexandre Tkatchenko. Machine learning for chemical discovery. *Nature Communications*, 11, 2020. URL https://api.semanticscholar.org/CorpusID:221137182.

Alexander Tropsha. Best practices for qsar model development, validation, and exploitation. *Molecular Informatics*, 29, 2010. URL https://api.semanticscholar.org/CorpusID:23564249.

Ashish Vaswani, Noam Shazeer, Niki Parmar, Jakob Uszkoreit, Llion Jones, Aidan N. Gomez, Lukasz Kaiser, and Illia Polosukhin. Attention is all you need. In Isabelle Guyon, Ulrike von Luxburg, Samy Bengio, Hanna M. Wallach, Rob Fergus, S. V. N. Vishwanathan, and Roman Garnett (eds.), *Advances in Neural Information Processing Systems 30: Annual Conference on Neural Information Processing Systems 2017, December 4-9, 2017, Long Beach, CA, USA*, pp. 5998–6008, 2017. URL https://proceedings.neurips.cc/paper/2017/hash/3f5ee243547dee91fbd053c1c4a845aa-Abstract.html.

Petar Velickovic, Guillem Cucurull, Arantxa Casanova, Adriana Romero, Pietro Liò, and Yoshua Bengio. Graph attention networks. In *6th International Conference on Learning Representations, ICLR 2018, Vancouver, BC, Canada, April 30 - May 3, 2018, Conference Track Proceedings*. OpenReview.net, 2018. URL https://openreview.net/forum?id=rJXMpikCZ.

Petar Velickovic, William Fedus, William L. Hamilton, Pietro Liò, Yoshua Bengio, and R. Devon Hjelm. Deep graph infomax. In *7th International Conference on Learning Representations, ICLR 2019, New Orleans, LA, USA, May 6-9, 2019*. OpenReview.net, 2019. URL https://openreview.net/forum?id=rklz9iAcKQ.

Aaron Virshup, Julia Contreras-García, Peter Wipf, Weitao Yang, and David N. Beratan. Stochastic voyages into uncharted chemical space produce a representative library of all possible drug-like compounds. *Journal of the American Chemical Society*, 135 19:7296–303, 2013. URL https://api.semanticscholar.org/CorpusID:10540378.

Sergei Voloboev. A review on fragment-based de novo 2d molecule generation, 2024. URL https://arxiv.org/abs/2405.05293.

W. Patrick Walters and Regina Barzilay. Applications of deep learning in molecule generation and molecular property prediction. *Accounts of chemical research*, 2020. URL https://api.semanticscholar.org/CorpusID:229715904.

Minjie Wang, Lingfan Yu, Da Zheng, Quan Gan, Yu Gai, Zihao Ye, Mufei Li, Jinjing Zhou, Qi Huang, Chao Ma, Ziyue Huang, Qipeng Guo, Hao Zhang, Haibin Lin, Junbo Zhao, Jinyang Li, Alexander J. Smola, and Zheng Zhang. Deep graph library: Towards efficient and scalable deep learning on graphs. *CoRR*, abs/1909.01315, 2019. URL http://arxiv.org/abs/1909.01315.

David Weininger. Smiles, a chemical language and information system. 1. introduction to methodology and encoding rules. *J. Chem. Inf. Comput. Sci.*, 28:31–36, 1988. URL https://api.semanticscholar.org/CorpusID:5445756.

Oliver Wieder, Stefan M. Kohlbacher, Mélaine A. Kuenemann, Arthur Garon, Pierre Ducrot, Thomas Seidel, and Thierry Langer. A compact review of molecular property prediction with graph neural networks. *Drug discovery today. Technologies*, 37:1–12, 2020. URL https://api.semanticscholar.org/CorpusID:230528669.

Tom Wollschläger, Niklas Kemper, Leon Hetzel, Johanna Sommer, and Stephan Günnemann. Expressivity and generalization: Fragment-biases for molecular gnns. In *Forty-first International Conference on Machine Learning, ICML 2024, Vienna, Austria, July 21-27, 2024*. OpenReview.net, 2024. URL https://openreview.net/forum?id=rPm5cKb1VB.

Olivier J. Wouters, Martin Mckee, and Jeroen Luyten. Estimated research and development investment needed to bring a new medicine to market, 2009-2018. *JAMA*, 323 9:844–853, 2020. URL https://api.semanticscholar.org/CorpusID:211834795.

Zhenqin Wu, Bharath Ramsundar, Evan N Feinberg, Joseph Gomes, Caleb Geniesse, Aneesh Pappu, Karl Leswing, and Vijay Pande. Moleculenet: A benchmark for molecular machine learning. *Chemical Science*, 9, 10 2017. doi: 10.1039/C7SC02664A.

Jun Xia, Chengshuai Zhao, Bozhen Hu, Zhangyang Gao, Cheng Tan, Yue Liu, Siyuan Li, and Stan Z. Li. Mole-bert: Rethinking pre-training graph neural networks for molecules. In *The Eleventh International Conference on Learning Representations, ICLR 2023, Kigali, Rwanda, May 1-5, 2023*. OpenReview.net, 2023. URL https://openreview.net/forum?id=jevY-DtiZTR.

Zhaoping Xiong, Dingyan Wang, Xiaohong Liu, Feisheng Zhong, Xiaozhe Wan, Xutong Li, Zhaojun Li, Xiaomin Luo, Kaixian Chen, Hualiang Jiang, and Mingyue Zheng. Pushing the boundaries of molecular representation for drug discovery with graph attention mechanism. *Journal of medicinal chemistry*, 2020. URL https://api.semanticscholar.org/CorpusID:199572628.

Keyulu Xu, Weihua Hu, Jure Leskovec, and Stefanie Jegelka. How powerful are graph neural networks? In *7th International Conference on Learning Representations, ICLR 2019, New Orleans, LA, USA, May 6-9, 2019*. OpenReview.net, 2019. URL https://openreview.net/forum?id=ryGs6iA5Km.

Minghao Xu, Hang Wang, Bingbing Ni, Hongyu Guo, and Jian Tang. Self-supervised graph-level representation learning with local and global structure. In Marina Meila and Tong Zhang (eds.), *Proceedings of the 38th International Conference on Machine Learning, ICML 2021, 18-24 July 2021, Virtual Event*, volume 139 of *Proceedings of Machine Learning Research*, pp. 11548–11558. PMLR, 2021. URL http://proceedings.mlr.press/v139/xu21g.html.

Ling Xue and Jürgen Bajorath. Molecular descriptors in chemoinformatics, computational combinatorial chemistry, and virtual screening. *Combinatorial chemistry & high throughput screening*, 3 5:363–72, 2000. URL https://api.semanticscholar.org/CorpusID:29690850.

Kevin Yang, Kyle Swanson, Wengong Jin, Connor W. Coley, Philipp Eiden, Hua Gao, Angel Guzman-Perez, Timothy Hopper, Brian Kelley, Miriam Mathea, Andrew Palmer, Volker Settels, Tommi S. Jaakkola, Klavs F. Jensen, and Regina Barzilay. Analyzing learned molecular representations for property prediction. *J. Chem. Inf. Model.*, 59(8):3370–3388, 2019. doi: 10.1021/ACS.JCIM.9B00237. URL https://doi.org/10.1021/acs.jcim.9b00237.

Chengxuan Ying, Tianle Cai, Shengjie Luo, Shuxin Zheng, Guolin Ke, Di He, Yanming Shen, and Tie-Yan Liu. Do transformers really perform badly for graph representation? In Marc'Aurelio Ranzato, Alina Beygelzimer, Yann N. Dauphin, Percy Liang, and Jennifer Wortman Vaughan (eds.), *Advances in Neural Information Processing Systems 34: Annual Conference on Neural Information Processing Systems 2021, NeurIPS 2021, December 6-14, 2021, virtual*, pp. 28877–28888, 2021. URL `https://proceedings.neurips.cc/paper/2021/hash/f1c1592588411002af340cbaedd6fc33-Abstract.html`.

Zhitao Ying, Dylan Bourgeois, Jiaxuan You, Marinka Zitnik, and Jure Leskovec. Gnnexplainer: Generating explanations for graph neural networks. In Hanna M. Wallach, Hugo Larochelle, Alina Beygelzimer, Florence d'Alché-Buc, Emily B. Fox, and Roman Garnett (eds.), *Advances in Neural Information Processing Systems 32: Annual Conference on Neural Information Processing Systems 2019, NeurIPS 2019, December 8-14, 2019, Vancouver, BC, Canada*, pp. 9240–9251, 2019. URL `https://proceedings.neurips.cc/paper/2019/hash/d80b7040b773199015de6d3b4293c8ff-Abstract.html`.

Yuning You, Tianlong Chen, Yongduo Sui, Ting Chen, Zhangyang Wang, and Yang Shen. Graph contrastive learning with augmentations. In Hugo Larochelle, Marc'Aurelio Ranzato, Raia Hadsell, Maria-Florina Balcan, and Hsuan-Tien Lin (eds.), *Advances in Neural Information Processing Systems 33: Annual Conference on Neural Information Processing Systems 2020, NeurIPS 2020, December 6-12, 2020, virtual*, 2020. URL `https://proceedings.neurips.cc/paper/2020/hash/3fe230348e9a12c13120749e3f9fa4cd-Abstract.html`.

Yuning You, Tianlong Chen, Yang Shen, and Zhangyang Wang. Graph contrastive learning automated. In Marina Meila and Tong Zhang (eds.), *Proceedings of the 38th International Conference on Machine Learning, ICML 2021, 18-24 July 2021, Virtual Event*, volume 139 of *Proceedings of Machine Learning Research*, pp. 12121–12132. PMLR, 2021. URL `http://proceedings.mlr.press/v139/you21a.html`.

Hongyang Yu and Hongjiang C. Yu. Tensorvae: a simple and efficient generative model for conditional molecular conformation generation. *Trans. Mach. Learn. Res.*, 2024, 2024. URL `https://openreview.net/forum?id=rQqzt4gYcc`.

Hao Yuan, Haiyang Yu, Jie Wang, Kang Li, and Shuiwang Ji. On explainability of graph neural networks via subgraph explorations. In Marina Meila and Tong Zhang (eds.), *Proceedings of the 38th International Conference on Machine Learning, ICML 2021, 18-24 July 2021, Virtual Event*, volume 139 of *Proceedings of Machine Learning Research*, pp. 12241–12252. PMLR, 2021. URL `http://proceedings.mlr.press/v139/yuan21c.html`.

Hao Yuan, Haiyang Yu, Shurui Gui, and Shuiwang Ji. Explainability in graph neural networks: A taxonomic survey. *IEEE Trans. Pattern Anal. Mach. Intell.*, 45(5):5782–5799, 2023. doi: 10.1109/TPAMI.2022.3204236. URL `https://doi.org/10.1109/TPAMI.2022.3204236`.

Xiangxiang Zeng, Hongxin Xiang, Linhui Yu, Jianmin Wang, KenLi Li, Ruth Nussinov, and Feixiong Cheng. Accurate prediction of molecular properties and drug targets using a self-supervised image representation learning framework. *Nature Machine Intelligence*, 4:1004–1016, 2022. URL `https://api.semanticscholar.org/CorpusID:253631433`.

Bingxu Zhang, Changjun Fan, Shixuan Liu, Kuihua Huang, Xiang Zhao, Jincai Huang, and Zhong Liu. The expressive power of graph neural networks: A survey. *CoRR*, abs/2308.08235, 2023. doi: 10.48550/ARXIV.2308.08235. URL `https://doi.org/10.48550/arXiv.2308.08235`.

Zaixi Zhang, Qi Liu, Hao Wang, Chengqiang Lu, and Chee-Kong Lee. Motif-based graph self-supervised learning for molecular property prediction. In Marc'Aurelio Ranzato, Alina Beygelzimer, Yann N. Dauphin, Percy Liang, and Jennifer Wortman Vaughan (eds.), *Advances in Neural Information Processing Systems 34: Annual Conference on Neural Information Processing Systems 2021, NeurIPS 2021, December 6-14, 2021, virtual*, pp. 15870–15882, 2021a. URL `https://proceedings.neurips.cc/paper/2021/hash/85267d349a5e647ff0a9edcb5ffd1e02-Abstract.html`.

Ziqiao Zhang, Jihong Guan, and Shuigeng Zhou. Fragat: a fragment-oriented multi-scale graph attention model for molecular property prediction. *Bioinform.*, 37(18):2981–2987, 2021b. doi: 10.1093/BIOINFORMATICS/BTAB195. URL `https://doi.org/10.1093/bioinformatics/btab195`.

Bolei Zhou, Aditya Khosla, Àgata Lapedriza, Aude Oliva, and Antonio Torralba. Learning deep features for discriminative localization. In *2016 IEEE Conference on Computer Vision and Pattern Recognition, CVPR 2016, Las Vegas, NV, USA, June 27-30, 2016*, pp. 2921–2929. IEEE Computer Society, 2016. doi: 10.1109/CVPR.2016.319. URL https://doi.org/10.1109/CVPR.2016.319.

Gengmo Zhou, Zhifeng Gao, Qiankun Ding, Hang Zheng, Hongteng Xu, Zhewei Wei, Linfeng Zhang, and Guolin Ke. Uni-mol: A universal 3d molecular representation learning framework. In *The Eleventh International Conference on Learning Representations, ICLR 2023, Kigali, Rwanda, May 1-5, 2023*. OpenReview.net, 2023. URL https://openreview.net/forum?id=6K2RM6wVqKu.

Jinhua Zhu, Kehan Wu, Bohan Wang, Yingce Xia, Shufang Xie, Qi Meng, Lijun Wu, Tao Qin, Wengang Zhou, Houqiang Li, and Tie-Yan Liu. O-gnn: incorporating ring priors into molecular modeling. In *The Eleventh International Conference on Learning Representations, ICLR 2023, Kigali, Rwanda, May 1-5, 2023*. OpenReview.net, 2023. URL https://openreview.net/forum?id=5cFfz6yMVPU.

A Proof of Theorem 1

Recall that $L^k(G)$ is the k-order line graph of G. Each vertex v in $L^k(G)$ corresponds to a $(k+1)$-size connected subgraph in G and we denote its node set by $C(v)$. We assume G is connected with more than k vertices.

Lemma 1. *Given a graph $G = (V, E)$, for every two adjacent nodes u, v in $L^k(G)$, we have $|C(u) \cap C(v)| \geq k$.*

Proof. Since u and v are adjacent in $L^k(G)$, they share a vertex in $L^{k-1}(G)$, which means they share a k-size connected subgraph in G. Thus, $|C(u) \cap C(v)| \geq k$. □

Theorem. *Given a graph $G = (V, E)$, the induced fragmentation of standard 0-overlapping fragmentation of $L^k(G)$ is a k-overlapping fragmentation of G.*

Proof. Denote the standard 0-overlapping fragmentation of $L^k(G)$ by $F = (P, A)$ and the induced fragmentation as $F' = (Q, A)$, where $P = \{U_i\}_{i=1}^m$, $\mathbf{A} \in \mathbb{R}^{m \times m}$, $Q = \{V_i\}_{i=1}^m$, $V_i = \bigcup\limits_{v \in U_i} C(v)$. We will prove that F' is a k-overlapping fragmentation of G.

1. $\bigcup\limits_{i=1}^{m} V_i = \bigcup\limits_{i=1}^{m} C(U_i) = V$, so Q is a vertex cover of G.

Since $G\left[U_i\right]$ is connected, and every two adjacent nodes in $L^k(G)$ share at least k nodes in G, so $G\left[V_i\right]$ is also connected.

Thus, F' is a fragmentation of G.

2. If $A_{ij} = 1$, then there exists $u_i \in U_i$ and $u_j \in U_j$, u_i and u_j are adjacent in $L^k(G)$. By Lemma 1, $|C(u_i) \cap C(u_j)| \geq k$. Thus,

$$|V_i \cap V_j| = \left|\left(\bigcup_{v \in U_i} C(v)\right) \cap \left(\bigcup_{v' \in U_j} C(v')\right)\right| = \left|\bigcup_{v \in U_i, v' \in U_j} C(v) \cap C(v')\right| \geq |C(u_i) \cap (u_j)| \geq k$$

Combining 1 and 2, we conclude F' is a k-overlapping fragmentation of G.

□

Disconnected Graph For a disconnected graph, we can apply the above theorem to each connected component. If a connected component contains only one node, we keep it unchanged in the line graph transformation.

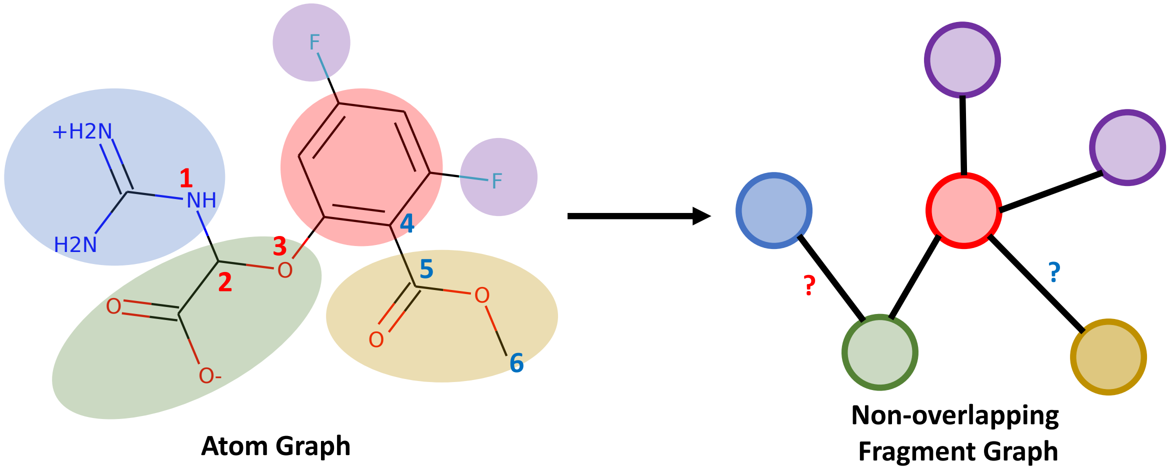

Figure 6: An example of connection information loss in non-overlapping fragmentation.

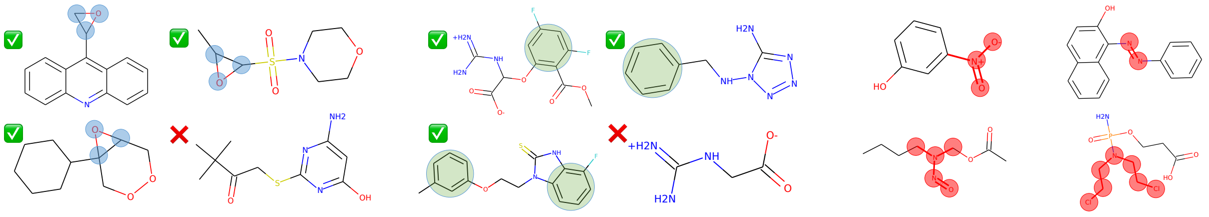

(a) (b) (c)

Figure 7: (a): 3MR dataset. The blue nodes indicate the 3MR substructure. The last molecule does not contain the 3MR substructure. (b) Benzene dataset. The green nodes indicate the benzene substructure. The last molecule does not contain the benzene substructure. (c) Mutagenicity dataset. The red nodes indicate the substructure alerts. All molecules are mutagenic in ames test.

B Connection Information Loss

We use an example to illustrate the connection information loss in the non-overlapping fragmentation. In Figure 6, we segment the molecule into six non-overlapping fragments and get the fragment graph. Within the fragment graph, the blue fragment is linked to the green fragment, but it's indistinguishable whether the connection is established through atom 1 and atom 2, or through atom 1 and atom 3. Similarly, the red fragment is connected with the yellow fragment, yet it remains unclear if this connection is formed by atom 4 and atom 5, or possibly atom 4 and atom 6. This specific kind of connection information is unfortunately lost within the context of a non-overlapping fragment graph. Based on our k-degree overlapping fragmentation, we can identify the connection information between fragments through the overlapping atoms. Since the connection information is preserved in the fragment graph, the model can access and *implicitly* utilize the connection information between fragments. We will explore more explicit ways to utilize the connection information in the future work.

C Interpretability Benchmark: DrugXAI

3MR 3MR dataset is a synthetic dataset that predicts the existence of 3MR substructure in the molecule. 3MR is a ring that consists of two carbon atoms and one oxygen atom, all connected by single bonds. The examples are given in Figure 7(a). The dataset is collected from ZINC15 lead-like subset and the ground truth attribution is the 3MR substructure.

Table 7: Dataset size of 3MR, Benzene and Mutagenicity.

	Train Set Size	Test Set Size
3MR	2521	631
Benzene	9600	2400
Mutagenicity	5204	1302

Table 8: Performance (AUROC) of CMPNN, GraphSAGE, GraphNet, GAT with CAM, GradCAM, GradInput, IG on 3MR dataset.

3MR	CMPNN	GraphSAGE	GraphNet	GAT
CAM	0.858	0.771	0.832	0.734
GradCAM	0.794	0.783	0.754	0.745
GradInput	0.951	0.844	**0.967**	0.877
IG	**0.966**	**0.932**	0.942	**0.905**
Best	0.966	0.932	0.967	0.905

Benzene Benzene dataset is a synthetic dataset designed to predict the presence of the benzene substructure within a molecule. Benzene is a ring consisting of six carbon atoms connected by aromatic bonds. The examples are illustrated in Figure 7(b). The dataset is also sourced from the ZINC15 lead-like subset, with the ground truth attribution being the benzene substructure.

Mutagenicity Mutagenicity dataset aims to predict the ames mutagenicity of molecules (Ames et al., 1973). We use the 46 substructure alerts from Sushko et al. (2012) as ground truth fragments.

The size of train and test set after dataset splitting are shown in Table 7. We report the test set attribution AUROC (McCloskey et al., 2019) of CMPNN, GraphSAGE, GraphNet, GAT with CAM, GradCAM, GradInput. in Table 8 (3MR dataset), Table 9 (Benzene datase), and Table 10 (Mutagenicity dataset). These results refer to DrugXAI (Rao et al., 2021). We list them here for the convenience of the reader.

Other Alternatives of FragCAM We adopt DeepLIFT (Shrikumar et al., 2017) and Integrated Gradients (IG) (Sundararajan et al., 2017) on the initial fragment vectors, which is the output of subgraph encoder, and denote these methods as FragDeepLIFT and FragIG. We set steps=50 for IG and use the default setting for DeepLIFT in Captum (Kokhlikyan et al., 2020). The results on DrugXAI are shown in Table 11 and Table 12. FragCAM outperforms FragDeepLIFT and FragIG on all datasets in terms of AUROC and fidelity, which demonstrates the effectiveness of FragCAM in explaining the prediction results with fragments.

D Experimental Details

Atom Features The composition of atom features is shown in Table 13.

Profile of PharmaBench The profile of the PharmaBench dataset is shown in Table 14.

Finetuning Details In the fine-tuning stage, we add a sum pooling on top of the pre-trained model and apply a linear predictor at last. We use Adam optimizer with a learning rate of $3e-5$ and a batch size of 32. We train the model for 50 epochs and report the mean performance on the test set over three runs with different random seeds. The model is implemented in DGL (Wang et al., 2019) with PyTorch (Paszke et al., 2019) as backend and trained on a single NVIDIA A800 GPU.

Time Measurement on Mutagenicity Dataset We measure the time per sample of FragCAM and SubgraphX on the mutagenicity dataset on a single NVIDIA 4090 GPU.

Table 9: Performance (AUROC) of CMPNN, GraphSAGE, GraphNet, GAT with CAM, GradCAM, GradInput, IG on Benzene dataset.

Benzene	CMPNN	GraphSAGE	GraphNet	GAT
CAM	0.831	0.798	0.859	0.776
GradCAM	0.566	0.582	0.657	0.604
GradInput	0.894	**0.859**	**0.934**	**0.867**
IG	**0.906**	0.801	0.865	0.798
Best	0.906	0.859	0.934	0.867

Table 10: Performance (AUROC) of Mutagenicity, GraphSAGE, GraphNet, GAT with CAM, GradCAM, GradInput, IG on Benzene dataset.

Mutagenicity	CMPNN	GraphSAGE	GraphNet	GAT
CAM	0.539	0.542	0.539	0.494
GradCAM	0.560	0.542	0.539	0.503
GradInput	0.607	0.607	0.654	0.608
IG	**0.742**	**0.742**	**0.759**	**0.683**
Best	0.742	0.742	0.759	0.683

E More Ablation Study on PharmaBench

Comparison between Different Fragmentation Hierarchies We first construct three hierarchy of fragmentation: All Atom, Junction Tree (JT) (Jin et al., 2018), and DOVE-1. "All Atom" takes each atom as a fragment. JT decomposes the molecule into rings and bonds. The number of fragments follows All Atom > JT > DOVE. We then evaluate the performance of FragFormer with different fragmentation methods, as shown in Table 15. The results show that the overall performance of FragFormer with DOVE is better than JT, which is better than All Atom.

Comparison between DOVE and JT-VAE JT-VAE (Jin et al., 2018) decomposes the molecule into rings and bonds. DOVE decomposes the molecule based on iterative line graph and principal subgraph mining (Kong et al., 2022). Compared with JT-VAE, DOVE can learn a succinct and expressive fragment library from molecule database by mining frequent substructures. The chemical functional groups in DOVE are more diverse and flexible than the rings and bonds in JT-VAE. Moreover, DOVE can decompose the molecule into fragments with tunable overlapping degree, which is not supported by JT-VAE. We constuct a baseline model called FragFormer-JT, which replace the DOVE with the Junction Tree fragmentation (JT-VAE) and keep all other settings the same. The results on PharmaBench are shown in Table 15. FragFormer-JT achieves lower performance than FragFormer on Pharmabench, which demonstrates the effectiveness of DOVE.

Comparison between Different k with the Same Vocabulary Vocabulary construction inherently depends on k, as it is performed on $L^k(G)$. We conduct an ablation experiment to isolate the difference of vocabulary. We first build the vocabulary for $k = 0, 1, 2, 3$ with vocab_size=500 and merge the vocabularies to get the final vocabulary. Then, we pre-train the model for $k = 0, 1, 2, 3$ with the final vocabulary separately and evaluate the performance on Pharmabench. The results are shown in Table 16. The optimal results for each dataset occur at $k = 1$ or $k = 2$, which is consistent with the findings in Table 1. Interestingly, under the same vocabulary, $k = 2$ yields superior performance more frequently than $k = 1$. The trend is reversed in Table 1.

Effect of Key Components Through an Incremental Ablation Study We begin with the baseline model, which employs mask atom prediction without incorporating knowledge fusion ('FragFormer-Atom w/o K'). Next, we introduce DOVE fragmentation with $k = 1$ ('FragFormer w/o K & Nested MFP'). Subsequently,

Table 11: Performance (AUROC) of FragCAM, FragIG, and FragDeepLift on DrugXAI.

Dataset/Method	FragCAM	FragIG	FragDeepLift
3MR	**0.981**	0.971	0.934
Benzene	**0.935**	0.886	0.875
Mutagenicity	**0.793**	0.711	0.704

Table 12: Fidelity(sparsity) of FragCAM, FragIG, and FragDeepLift on DrugXAI.

Dataset/Method	FragCAM	FragIG	FragDeepLift
3MR	**0.87(0.85)**	0.87(0.78)	0.13(0.75)
Benzene	**0.50(0.67)**	0.46(0.64)	0.45(0.64)
Mutagenicity	**0.35(0.72)**	0.36(0.67)	0.19(0.66)

we incorporate the nested MFP pre-training criterion ('FragFormer w/o K'). Finally, we enhance the model by adding the knowledge fusion layer ('FragFormer'). The results are shown in Table 17. Each component contributes to the performance improvement.

F Results on MoleculeNet

We test FragFormer (DOVE-1) on the MoleculeNet benchmark (Wu et al., 2017). We follow the experimental settings in KPGT (Li et al., 2023). We split the dataset into 80% training, 10% validation, and 10% test with scaffold splitting. We report the mean performance over three runs with different random splits. The results are shown in Table 18. All baseline results of atom-based models are taken from KPGT. FragFormer outperforms all fragment-based baselines and achieves the SOTA performance on 7 out of 11 datasets. We find that FragFormer excels at the target-related tasks, e.g., BBBP, BACE, Estrogen, while underperforms previous SOTA method on toxicity-related tasks, e.g., Tox21, ToxCast. We hypothesize that this could be due to differences in task characteristics, and we plan to investigate the underlying reasons for this phenomenon in future work.

Table 13: Composition of atom features.

Feature Description	Feature Dimension
One hot encoding for the atom type, e.g., C, N, O	101
One hot encoding for the atom degree	12
Formal charge	1
One hot encoding for radical electrons	6
One hot encoding for atom hybridization	6
Whether the atom is in aromatic ring	1
One hot encoding of number of H	6
Whether the atom is chiral center	1
One hot encoding of chirality type	2
normalized atom mass	1

Table 14: Datasets Profile for PharmaBench.

Dataset Name	Dataset Size	Task Type	Category	Task Description
AMES	9,139	classification	Toxicity	The result of AMES test (Ames et al., 1973) which evaluates the mutagenic potential of the molecule.
BBB	8,301	classification	Absorption	Predict the Blood-Brain Barrier (BBB) penetration. The dataset is labeled according to threshold $\log \mathrm{BB} = -1$.
CYP2C9	999	regression	Metabolism	Binding affinity to CYP2C9 (unit: $\log 10\mu M$).
CYP2D6	1,214	regression	Metabolism	Binding affinity to CYP2D6 (unit: $\log 10\mu M$).
CYP3A4	1,980	regression	Metabolism	Binding affinity to CYP3A4 (unit: $\log 10\mu M$).
HLMC	2,286	regression	Clearance	The clearance speed in the liver microsomal system in human (unit: $\log 10$(mL/min/g)).
MLMC	1,403	regression	Clearance	The clearance speed in the liver microsomal system in mouse (unit: $\log 10$(mL/min/g)).
RLMC	1,129	regression	Clearance	The clearance speed in the liver microsomal system in rat (unit: $\log 10$(mL/min/g)).
LogD	13,068	regression	Physochemical	LogD is the logarithm of the distribution coefficient (D), which measures PH-adjusted lipophilicity of the molecule.
PPB	1,262	regression	Distribution	Percentage of the molecule in the plasma that is bound.
Sol	11,701	regression	Physochemical	Water solubility of the molecule (unit: $\log 10nM$).

Table 15: Comparison between different hierarchy of fragmentation.

	Classfication (AUROC ↑)		Regression (RMSE ↓)								
Method/Dataset	AMES	BBB	CYP2C9	CYP2D6	CYP3A4	HLMC	MLMC	RLMC	LogD	PPB	Sol
FragFormer-Atom	0.867	0.916	17.849	16.133	16.663	0.606	0.755	0.718	0.800	0.192	1.045
FragFormer-JT	0.863	0.919	17.413	15.666	16.603	0.550	0.746	0.711	0.709	0.185	0.938
FragFormer-DOVE	**0.889**	**0.927**	**16.855**	**14.425**	**15.894**	**0.514**	**0.702**	**0.596**	**0.667**	**0.157**	**0.895**

Table 16: Comparison between different overlapping degree k with the same vocabulary.

	Classfication (AUROC ↑)		Regression (RMSE ↓)								
Method/Dataset	AMES	BBB	CYP2C9	CYP2D6	CYP3A4	HLMC	MLMC	RLMC	LogD	PPB	Sol
FragFormer-0	0.858	0.918	17.358	17.241	16.859	0.625	0.854	0.603	0.780	0.193	0.952
FragFormer-1	0.865	**0.922**	17.316	14.833	15.773	**0.517**	0.734	0.565	0.695	**0.175**	0.910
FragFormer-2	**0.870**	0.920	**16.732**	**14.538**	**15.302**	0.519	**0.708**	**0.548**	**0.687**	0.177	**0.905**
FragFormer-3	0.860	0.917	17.809	16.986	16.910	0.544	0.754	0.577	0.725	0.199	0.959

Table 17: Effect of key components.

	Classfication (AUROC ↑)		Regression (RMSE ↓)								
Method/Dataset	AMES	BBB	CYP2C9	CYP2D6	CYP3A4	HLMC	MLMC	RLMC	LogD	PPB	Sol
FragFormer-Atom w.o K	0.837	0.913	18.264	16.691	17.190	0.620	0.996	0.937	0.894	0.236	1.387
FragFormer w.o (K&Nested MFP)	0.856	0.921	17.919	15.659	16.894	0.563	0.877	0.774	0.740	0.211	1.134
FragFormer w.o K	0.882	0.921	17.851	14.815	16.055	**0.512**	0.799	0.680	0.706	0.166	0.981
FragFormer	**0.889**	**0.928**	**16.855**	**14.425**	**15.894**	0.514	**0.702**	**0.596**	**0.667**	**0.157**	**0.895**

Table 18: Results on MoleculeNet. Baselines labeled with "†" are fragment-based methods.

Method	Classification (AUROC ↑)								Regression (RMSE ↓)		
	BACE	BBBP	ClinTox	SIDER	Estrogen	MetStab	Tox21	ToxCast	FreeSolv	ESOL	Lipo
Infomax (Velickovic et al., 2019)	0.839	0.840	0.661	0.616	0.888	0.837	0.816	0.690	4.119	1.462	0.978
Edgepred (Hamilton et al., 2017b)	0.817	0.873	0.730	0.603	0.881	0.844	0.818	0.712	3.849	2.272	1.030
Masking (Hu et al., 2020)	0.823	0.864	0.729	0.573	0.869	0.868	0.798	0.663	3.646	2.100	1.063
Contextpred (Hu et al., 2020)	0.840	0.877	0.732	0.609	0.882	0.857	0.806	0.714	3.141	1.349	0.969
Infomax_sup (Hu et al., 2020)	0.839	0.873	0.754	0.622	0.864	0.864	0.826	0.713	3.017	1.238	0.729
Edgepred_sup (Hu et al., 2020)	0.847	0.859	0.745	0.620	0.890	0.852	0.829	0.721	2.889	1.133	0.707
Masking_sup (Hu et al., 2020)	0.824	0.859	0.796	0.606	0.888	0.872	0.827	0.715	3.210	1.387	0.725
Contextpred_sup (Hu et al., 2020)	0.855	0.875	0.802	0.620	0.885	0.859	0.840	0.724	3.105	1.477	0.754
GraphLoG (Xu et al., 2021)	0.830	0.846	0.667	0.615	0.871	0.850	0.796	0.677	4.174	2.335	1.104
GraphCL (You et al., 2020)	0.825	0.887	0.691	0.587	0.875	0.821	0.805	0.696	4.014	1.835	0.945
JOAO (You et al., 2021)	0.826	0.879	0.741	0.640	0.861	0.837	0.823	0.711	3.466	1.771	0.933
GROVER (Rong et al., 2020)	0.840	0.887	0.874	0.638	0.892	0.876	0.838	0.696	2.991	0.928	0.752
3DInfomax (Stärk et al., 2022)	0.811	0.877	0.887	0.585	0.880	0.866	0.805	0.716	2.919	1.906	1.045
GraphMVP (Liu et al., 2022)	0.818	0.860	0.719	0.584	0.865	0.820	0.799	0.689	2.532	1.937	0.990
MolFormer (Ross et al., 2021)	0.791	0.866	0.810	0.578	0.806	0.651	0.764	0.687	2.322	0.821	0.673
ImageMol (Zeng et al., 2022)	0.786	0.881	0.885	0.625	0.839	0.874	0.816	0.710	2.634	1.869	0.765
GEM (Fang et al., 2021)	0.857	0.895	0.905	0.621	0.894	0.863	0.832	0.733	2.389	0.803	0.663
GraphMAE (Hou et al., 2022)	0.857	0.878	0.748	0.597	0.881	0.853	0.801	0.691	3.023	1.378	0.746
MoleBERT (Xia et al., 2023)	0.843	0.851	0.797	0.615	0.887	0.868	0.832	0.720	2.801	1.185	0.690
KPGT (Li et al., 2023)	0.855	0.908	**0.946**	0.649	0.905	0.889	**0.848**	**0.746**	2.121	0.803	**0.600**
GraphFP† (Luong & Singh, 2023)	0.839	0.869	0.832	0.598	0.879	0.857	0.813	0.707	3.228	1.805	0.803
FraGAT† (Zhang et al., 2021b)	0.813	0.841	0.726	0.577	0.867	0.841	0.771	0.682	4.049	2.043	0.913
PharmHGT† (Jiang et al., 2023)	0.846	0.891	0.895	0.625	0.892	0.874	0.824	0.715	2.411	1.276	0.779
FragFormer†	**0.868**	**0.912**	0.919	**0.656**	**0.918**	**0.894**	0.840	0.732	**1.990**	**0.801**	0.642